Sensitivity of interfacial hydraulics to the microtopographic roughness of water-lain gravels

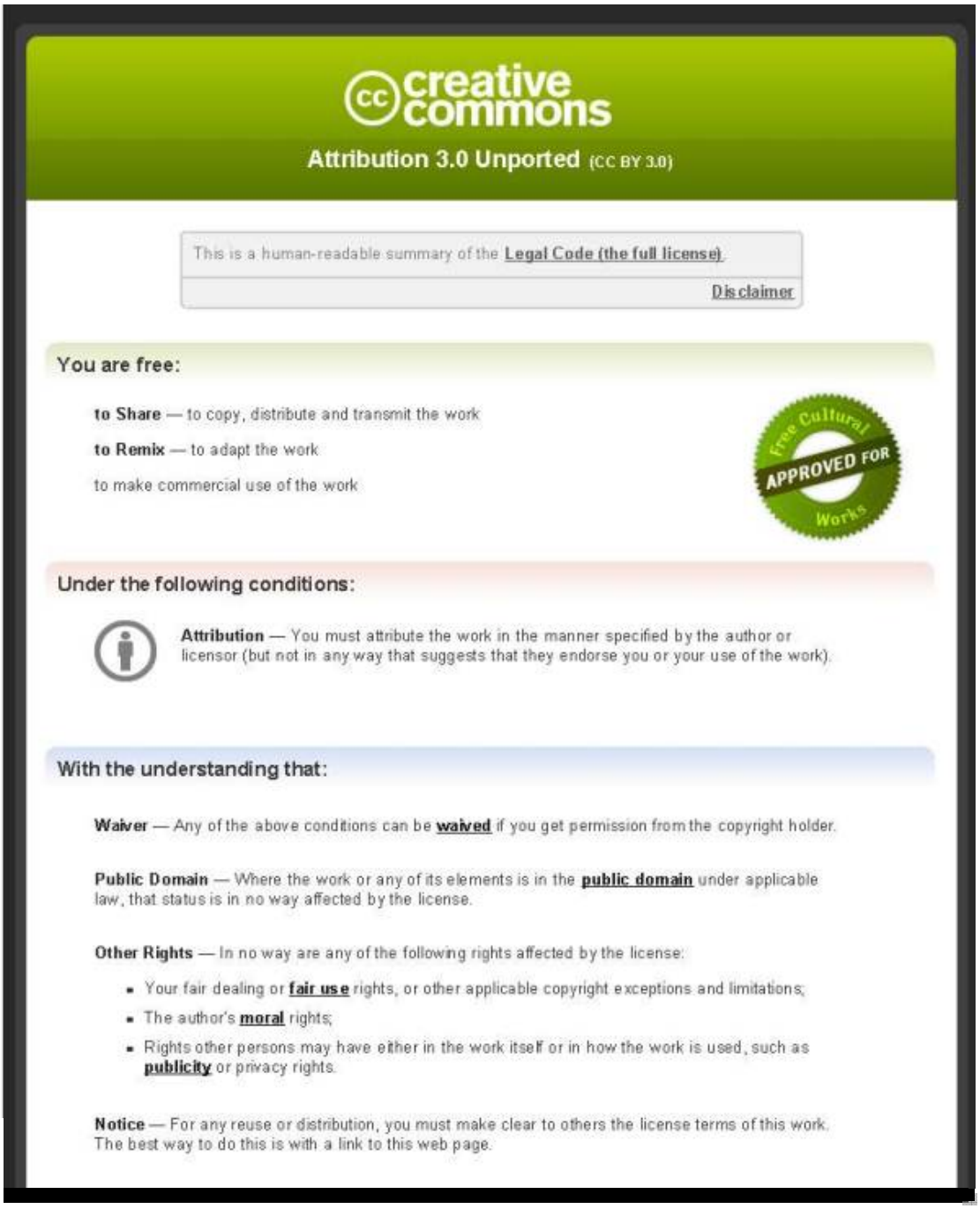

EARTH SURFACE PROCESSES AND LANDFORMS
Earth Surf. Process. Landforms **39**, 184–199 (2014)

Published online 24 June 2013 in Wiley Online Library
(wileyonlinelibrary.com) DOI: 10.1002/esp.3438

Sensitivity of interfacial hydraulics to the microtopographic roughness of water-lain gravels

Stephen P. Rice,[1]* Thomas Buffin-Bélanger[2] and Ian Reid[1]
[1] Centre for Hydrological and Ecosystem Science, Loughborough University, Loughborough LE11 3TU, UK
[2] Groupe de Recherché sur les Environments Nordiques, Université du Québec à Rimouski, Canada

Received 3 August 2012; Revised 27 March 2013; Accepted 17 April 2013

*Correspondence to: S. Rice, Centre for Hydrological and Ecosystem Science, Loughborough University, Loughborough, LE11 3TU, UK. E-mail: s.rice@lboro.ac.uk

ESPL
Earth Surface Processes and Landforms

ABSTRACT: Flow within the interfacial layer of gravel-bed rivers is poorly understood, but this zone is important because the hydraulics here transport sediment, generate flow structures and interact with benthic organisms. We hypothesized that different gravel-bed microtopographies generate measurable differences in hydraulic characteristics within the interfacial layer. This was tested using a high density of spatially and vertically distributed, velocity time series measured in the interfacial layers above three surfaces of contrasting microtopography. These surfaces had natural water-worked textures, captured in the field using a casting procedure. Analysis was repeated for three discharges, with Reynolds numbers between 165000 and 287000, to evaluate whether discharge affected the impact of microtopography on interfacial flows. Relative submergence varied over a small range (3.5 to 8.1) characteristic of upland gravel-bed rivers. Between-surface differences in the median and variance of several time-averaged and turbulent flow parameters were tested using non-parametric statistics. Across all discharges, microtopographic differences did not affect spatially averaged (median) values of streamwise velocity, but were associated with significant differences in its spatial variance, and did affect spatially averaged (median) turbulent kinetic energy. Sweep and ejection events dominated the interfacial region above all surfaces at all flows, but there was a microtopographic effect, with Q2 and Q4 events less dominant and structures less persistent above the surface with the widest relief distribution, especially at the highest Reynolds number flow. Results are broadly consistent with earlier work, although this analysis is unique because of the focus on interfacial hydraulics, spatially averaged 'patch scale' metrics and a statistical approach to data analysis. An important implication is that observable differences in microtopography do not *necessarily* produce differences in interfacial hydraulics. An important observation is that appropriate roughness parameterizations for gravel-bed rivers remain elusive, partly because the relative contributions to flow resistance of different aspects of bed microtopography are poorly constrained. © 2014 The Authors. Earth Surface Processes and Landforms Published by John Wiley & Sons Ltd.

KEYWORDS: interfacial layer; gravel-bed roughness; quadrant analysis; coherent flow structure; near-bed hydraulics; sediment patch

Introduction

In gravel-bed rivers there is a near-bed region where spatial and temporal hydraulic variations are dominated by the local interaction of the flow with heterogeneous grain roughness; that is, with the grain-scale bed microtopography. This region extends from slightly above the grain tops to the base of the grain troughs and has been referred to as the inner region by Nowell and Church (1979), the inner zone by Kirkbride (1993) and the roughness layer by Nikora *et al*. (2001, 2004). The distinguishing characteristic of this region is that flows are directly affected by the contingent configuration of the boundary grains, whereas the logarithmic flow region above it reflects only the macroscopic effects of that roughness integrated across time and space (Ferreira *et al*., 2010). Specifically, and adopting Nikora *et al*.'s (2001) nomenclature (their Figure 2, p. 125), the roughness layer has two components: the interfacial sublayer between the roughness troughs and tops where form drag operates; and the form-induced sublayer that lies just above the roughness tops where flow separation off bed-particle crests dominates the generation of stresses.

Knowledge of flow characteristics within the interfacial layer of gravel-bed rivers, and the roughness layer in general, is limited compared with understanding of velocity and turbulence structure in the main body of the flow, probably because of the relative difficulty of making detailed measurements close to the bed. Interfacial hydraulics are poorly understood both within deep flows over relatively fine gravel beds and for relatively shallow flows over coarse beds (Nikora *et al*., 2001; Sarkar and Dey, 2010). This is despite a general expectation that the hydraulic forces in this region, including turbulent structures, are important for the dynamics of sediment transport and the formation of bed forms (Cleaver and Yates, 1976; Drake *et al*., 1988; Nelson *et al*., 1995; Nino and Garcia, 1996; Schmeeckle *et al*., 2007; Paiement-Paradis *et al*., 2011; Cooper, 2012), it is in this region where skin friction and form drag contribute to the momentum balance and it is here that the turbulence structures of the boundary layer are generated

(Kirkbride, 1993; Robert, 1993; Papanicolaou *et al.*, 2001; Hardy *et al.*, 2009; Marquis and Roy, 2011). This is also the region of the flow where benthic species live, so that near-boundary hydraulics is an important element of the physical habitat template in gravel-bed rivers (Nowell and Jumars, 1984; Davis and Barmuta, 1989; Lancaster, 1999; Jowett, 2003; Rice *et al.*, 2008). Grain sorting at a variety of scales produces spatially patchy bed surface textures, so that sub-width to width-scale microtopographic variability is a fundamental feature of gravel-bed rivers. Appreciating the interactions between sediment patches and near-bed flows is important for a host of gravel- bed river processes and phenomena including sediment sorting and bed load transport (Bluck, 1987; Clifford *et al.*, 1993; Garcia *et al.*, 2007), lotic habitat distribution (Crowder and Diplas, 2000; Brooks *et al.*, 2005; Tritico and Hotchkiss, 2005; Oldmeadow *et al.*, 2010), structure of the flow (Clifford *et al.*, 1992; Robert *et al.*, 1992; Lawless and Robert, 2001a) and the generation of coherent flow structures (Hardy *et al.*, 2010; Casas *et al.*, 2010).

This paper considers flow characteristics within the interfacial layer above water-worked gravel beds and evaluates the impact of contrasting patch-scale bed microtopography on the spatial distribution (average response and spatial variability) of hydraulic properties throughout the interfacial layer volume.

Background and Aims

Numerous field studies have captured information about interactions between surface roughness and roughness layer hydraulics in wadeable gravel-bed rivers where relative submergence is low. This work has focused on characterizing time-averaged properties and turbulent structures associated with isolated roughness elements like pebble clusters (Buffin-Belanger and Roy, 1998; Tritico and Hotchkiss, 2005; Lacey and Roy, 2007; Strom and Papanicolaou, 2007), on the impact of relatively homogeneous roughness on turbulent properties (Papanicolaou *et al.*, 2001; Franca *et al.*, 2008), or on understanding the scales of turbulence and their association with particular roughness features (Clifford, 1996; Roy *et al.*, 2004; Lacey and Roy, 2008; Marquis and Roy, 2011). Most of this field work and relevant flume studies (Nowell and Church, 1979; Lawless and Robert, 2001b; Canavaro *et al.*, 2007; Strom *et al.*, 2007) necessarily employed a relatively small number of closely located vertical profile measurements to accumulate information about the flow field.

Recently, the application of particle imaging velocimetry (PIV) in flume experiments has permitted examination of the near-bed velocity field in greater spatial detail, especially in planes. Of specific interest is the work of Sambrook Smith and Nicholas (2005) and Hardy *et al.* (2009, 2010) who explicitly examined the impact of systematic changes in gravel-bed roughness on near-bed flow properties and the generation of coherent flow structures. Both focused on vertical, streamwise planes that included a slice of the interfacial layer. Sambrook Smith and Nicholas (2005) simulated gravel beds using a two-dimensional concrete model (no variation in cross-stream elevation) based on a bed profile from the Allt Dubhaig, Scotland and smoothed this roughness by filling the troughs with increasing amounts of flooring compound. They noted that reduced roughness was associated with an increase in near-bed streamwise velocity, a reduction in turbulent kinetic energy and shear stress and a decline in the incidence of high magnitude quadrant 2 (ejection) and quadrant 4 (sweep) events. Hardy *et al.* (2009, 2010) water worked a gravel bed then added successive amounts of sand to it in order to obtain beds of different microtopographic roughness. High resolution vertical maps of time average flow fields, of instantaneous flow fields, of turbulence intensity, and of quadrant and wavelet power spectra were produced and analysed. They found that reduced roughness was associated with a weakening of coherent flow structures in the body of the flow (Hardy *et al.*, 2010) and concluded that coherent flow structures over gravels originate in bed-generated turbulence associated with a combination of flow separation around large upstanding clasts and Kelvin–Helmholtz instabilities generated within the wake layer (Nowell and Church, 1979) by wake flapping (Hardy *et al.*, 2009, 2010).

Relatively little work on the interactions between gravel roughness and depth-limited flow hydraulics has included spatially distributed measurements of *planimetric variability*, even though the lateral and longitudinal spatial organization of hydraulic parameters close to the bed is of particular relevance given the patchy, heterogeneous nature of the grain-composed boundary of gravel-bed rivers – in terms of grain sizes, grain structuring, grain shapes and grain agglomeration. Attempts to develop rigorous and feasible means of simulating three-dimensional flow fields using computational fluid dynamics (CFD) have used spatially distributed flume measurements to validate numerical outputs (Lane *et al.*, 2004; Hardy *et al.*, 2007; Strom *et al.*, 2007) and both observations and modelling have provided information about the interfacial layer, not least in the form of visualizations of numerical output that reveal important features of the interaction between the flow and the boundary. In the field, Lamarre and Roy (2005) and Legleiter *et al.* (2007) obtained spatially-distributed measurements in channels with low relative depth and asked how spatial variations in velocity and turbulence characteristics are related to the spatial distribution of roughness elements under different flow depths. Both studies found that local microtopography had only local impacts on flow characteristics, which diminished as flow depth increased, and that reach-scale flow properties were controlled, instead, by differences in flow depth. In a comparable series of flume experiments, Cooper and Tait (2008) used PIV to obtain high resolution spatial measurements of time-averaged streamwise velocity in several horizontal sheets above two water-worked gravel beds; these lay a short distance above the highest bed elevations, within the form-induced sublayer. They examined the spatial organization of streamwise velocity in relation to grain-scale bed surface topography and relative submergence, and reached the same conclusion as the field studies, that relative submergence was a much stronger control on velocity variations above both experimental surfaces.

Nikora *et al.* (2004) compiled a set of data from eight laboratory studies in which there was an emphasis on examining flow properties within the interfacial layer. The reported experiments mostly used unnatural roughness elements (beads, cubes, triangular bars) but also included one study that used rounded, crushed and natural gravels (Sumer *et al.*, 2001) and one that used well-rounded, narrowly graded gravels in a single layer (Dittrich and Koll, 1997). Subsequent additions to this body of work now include Sarkar and Dey (2010) and Mignot *et al.* (2009) who examined 'double averaged' (DA) turbulence characteristics (e.g. Reynolds shear stresses, quadrant analysis and turbulent kinetic energy budget) within and above the interfacial layers of non-worked beds of uniform rounded gravel ($D_{50} = 25$ mm) and a non-worked bed of uniform angular stones ($D_{50} = 20$ mm), respectively.

The field and flume work cited above has provided valuable insights into the role of surface roughness in affecting roughness layer hydraulics but this has been based on data from a relatively limited number of spatially distributed profiles, from vertical planes or from experiments utilizing unnatural roughness. Moreover, relatively little of this work has focused explicitly on the interfacial zone. In this work we examine interfacial flows above naturally water-worked gravel beds, but with an emphasis on capturing the spatial and temporal variability of hydraulic properties within the interfacial volume. In a previous paper

(Buffin-Bélanger *et al.*, 2006), we examined the spatial heterogeneity and mean response of several flow properties within and above the interfacial layer of a single water-lain gravel surface, under three different discharges. In that paper we asked the question: 'How do spatial and temporal parameters of the near bed hydraulics field change as discharge increases over a particular gravel bed?' The near-bed region was defined as the interfacial sublayer plus the form-induced sublayer (that is the entire roughness layer). We found that Reynolds number and local elevation of the data-averaging layer were important controls on the mean (time and space averaged) response and spatial heterogeneity of flow properties including turbulent kinetic energy and streamwise and vertical velocity. Like Mignot *et al.* (2009), who examined near-boundary flows above random arrangements of angular gravels, and Hardy *et al.* (2009, 2010), who examined the near-bed flow region in a vertical plane above three gravel surfaces of variable roughness, we found that maximum turbulence intensity occurred on the lee side of particle crests, where shear layers bound separated flow and shed vortices (Buffin-Bélanger *et al.*, 2006). We also observed that this layer of intense turbulence was depressed toward the bed as discharge and Reynolds number increased, suggesting that lee-side separation zones are flattened as the ambient flow strength increases.

This present work is concerned with a related but very different question: 'To what extent are the spatial and temporal characteristics of flows within the interfacial sublayer affected by the microtopography of the bed surface?' This is a legitimate question because it informs us about how near-bed flows of importance for grain entrainment, benthic organisms and flow resistance may vary between different gravel patches, facies, or mesohabitats. Sambrook-Smith and Nicholas (2005) and Hardy *et al.* (2009, 2010) have asked similar questions about how systematic changes in surface microtopography and flow strength affect near-bed flow properties and the generation of coherent flow structures in depth-limited flows above gravel-bed surfaces. We hypothesize that different gravel-bed microtopographies generate measurable differences in hydraulic variables within the roughness layer; specifically, differences in (1) the central tendency and (2) the variance of spatial distributions. In the absence of empirical or theoretical evidence to the contrary, these hypotheses are legitimate points of departure. The hypotheses are tested by comparing interfacial flow characteristics throughout the volume of the interfacial layers above each of three water-lain gravel beds of contrasting roughness, where the differences in roughness between the beds are sufficient to expect an impact on integral flow characteristics in the boundary layer as a whole. It is then possible to also comment on how the macroscopic roughness effect on boundary-layer flow characteristics relate to the microtopographic effects of roughness in the interfacial layer. These analyses were repeated for three discharges to examine whether and how the gross flow condition affects any microtopographic impacts on interfacial flow. There are some key differences with Buffin-Bélanger *et al.* (2006): (1) our earlier paper considered three experiments (one microtopography, three discharges), but here we present results for nine experiments (three microtopographies, three discharges); and (2) only flows within the interfacial layer (rather than the entire roughness layer) are considered. The data used herein is mostly unreported (data for two of the three gravel-bed facsimiles) but some of the data is a subset (interfacial layer only) of that used to examine discharge effects on the roughness layer above the third gravel-bed facsimile in Buffin-Belanger *et al.* (2006).

A selection of hydraulic variables of specific interest is considered. A time-averaged flow parameter (mean streamwise velocity, $\overline{u}$) and dynamic flow property (turbulent kinetic energy, K) are examined because they provide basic information about the flow that affects sediments and organisms found in the interfacial layer. Standard measures of flow coherence or structure are also examined because they provide insight into how the flow is organized through time within the interfacial layer. We focus on quadrant and autocorrelation analysis of u (streamwise) and v (vertical) time series to derive the proportion of time within quadrants *Q1* (outward interaction), *Q2* (ejection), *Q3* (inward interaction) and *Q4* (sweep) and to determine two measures of structural coherence (the u-series time scale *TS* and the integral time scale *ITS*). In addition, we examine whether any detected differences in these hydraulic measurements can be explained by two key contrasts in the characteristics that define the microtopographic roughness of the three surfaces examined: specifically, differences in particle roundness and differences in surface elevation distributions.

Methods

Experimental surfaces

We used a casting procedure to produce accurate three-dimensional facsimiles of three water-lain, fluvial gravel beds (Buffin-Bélanger *et al.*, 2003). Controlled observations above such natural fabrics are difficult to achieve in the field and become impracticable at high flows. Conversely, control of flow properties is possible in laboratory flumes but the reproduction of natural fabrics for the cobble–gravel sizes we investigated requires greater transport rates than can be generated routinely (cf. Cooper and Tait, 2009). Instead, many flume experiments have utilized simulated gravel mixtures and idealized roughness elements (Grass, 1971; Nowell and Church, 1979; Robert *et al.*, 1992; Kirkbride, 1993; Dancey *et al.*, 2000), or have tried to import or reconstruct natural bed configurations (Young, 1992; Buffin-Bélanger, 2001; Lawless and Robert, 2001b). The casts used here are impermeable which means that there is no exchange of water with the bed, as in a natural channel.

The casts each measured 2.0 by 1.0 m and were obtained from texturally homogeneous gravel–cobble units on exposed gravel bars in the River Lune, Lancashire, UK (cast 2) and the River Manifold in Derbyshire, UK (casts 3 and 4). Note that cast 1 is not used in this paper, but we retain this nomenclature for easy comparison with other published work. In our previous paper (Buffin-Bélanger *et al.*, 2006) we used cast 2. The three surfaces were visually selected to represent differences in roughness as a function of variations in particle size, surface elevation distribution and roundness: specifically, casts 3 and 4 were selected for their similar roundness but distinctive elevation distributions, and casts 2 and 4 for their similar elevations but distinctive roundness (further details below). On each cast, a representative sub-area measuring 0.8 m in x (streamwise) and 0.5 m in y (cross-stream) was selected for detailed investigation (Figure 1).

Digital elevation models of each sub-area were generated with a grid resolution of 0.005 m by close-range digital photogrammetry (Chandler *et al.*, 2003). Elevation data are similar to those of gravel beds documented in the field with lognormal distributions that are consistent with the six natural river gravels described by Smart *et al.* (2002). Skewness values of the three elevation distributions (0.6, 0.5, 1.3, respectively) are similar to an average value reported by Nikora *et al.* (1998) for 77 field profiles from eight gravel-bed rivers (0.5, standard deviation 0.5) and notably different from the negative skewness values reported for artificial, 'unworked' flume beds by Kirchner *et al.* (1990). The scaling properties of variations in elevation across the cast are also realistic. An omni-directional semivariogram for each sub-area was constructed from the digital elevation data for lags less than one-third of the diagonal distance across the measured area

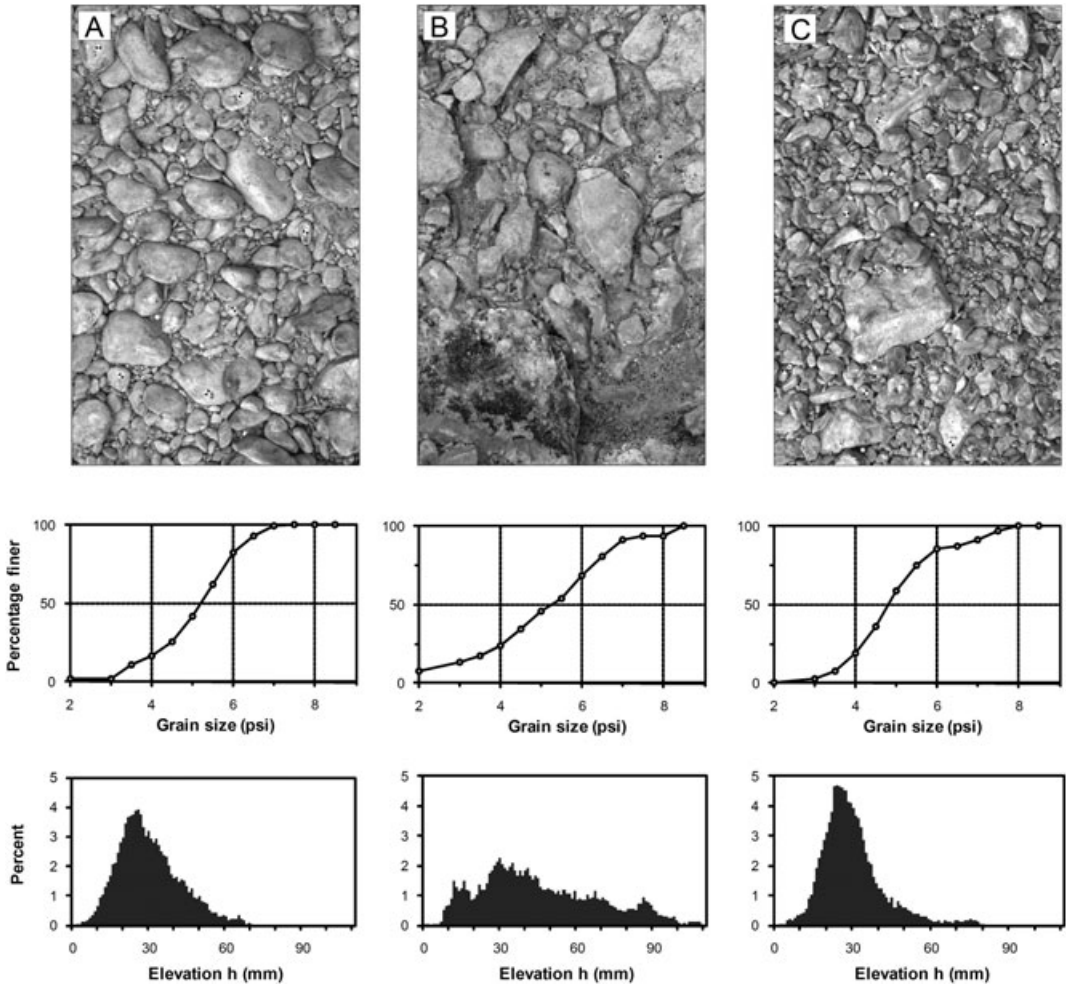

Figure 1. Orthophotographs and roughness characteristics of the detailed measurement areas on the three casts. Each image is of an area 0.8 m in *x* (streamwise) and 0.5 m in *y* (cross-stream) and in each case flow would be from top to bottom: (A) cast 2 from the River Lune, England; (B) cast 3 and (C) cast 4, both from the River Manifold, England. Cumulative grain size and surface elevations distributions (for heights measured relative to the lowest point of the surface, z_{min}) are shown beneath the respective orthophotographs.

(< 0.31 m). In each case, the two-dimensional, streamwise semivariogram was extracted, in which empirical semivariance is calculated for all pairs of points in the streamwise direction at all cross-stream positions. Log-log plots of semivariance against lag share common diagnostic features (two linear facets with typical slope values separated by breakpoints that approximate the D_{50} grain size) with those reported for natural gravel beds (Robert, 1988, 1990; Singsabaugh *et al.*, 1991; Nikora *et al.*, 1998) and water worked beds in sediment-fed flume experiments with small gravels (Cooper and Tait, 2009).

A grain size distribution for each patch was obtained, but to preserve bed fabric, direct grain-size sampling of the prototype cast area (in the field) was avoided. Instead, b-axis measurements were made from the finished casts using a 0.1 by 0.1 m grid to collect a Wolman sample of approximately 170 measurements in each case. Despite the inability to manipulate individual clasts we are confident that this method produced reasonable grain size statistics. For cast 2, 11 paint-and-pick grain-size samples were collected from the same homogeneous gravel–cobble unit as the cast. When converted to grid-by-number equivalents with the same lower truncation (4 mm), these yield average D_{50}, D_{84} and D_{95} values of 33, 68 and 97 mm, respectively. These compare very well with the values obtained from the finished cast (37, 68 and 99 mm) and demonstrate that sampling from the finished casts yields acceptable grain-size data.

The two casts from the River Manifold were collected within a few km of each other and the constituent grains are similar in shape and roundness. The relatively angular particles reflect the immaturity of the carboniferous limestone bed material, which is mainly derived from local cliffs and exposures in the channel bed (Figure 1). However, the size characteristics of the two casts are very different: cast 3 is less well sorted than cast 4 ($\sigma_D = (\Psi_{84} - \Psi_{16})/2$, where Ψ indicates a b-axis percentile on the Psi scale, of 1.7 and 1.0, respectively) and contains substantially larger grains, with a D_{84} of 100 mm compared with 61 mm (Figure 1). There are corresponding differences in bed elevation with cast 3 differentiated by a standard deviation $\sigma_h = 23$ mm, that is almost twice that of cast 4 ($\sigma_h = 12$ mm), and a median elevation (41 mm) that is 13 mm higher than on cast 4 (Figure 1). In contrast, the elevation distributions of casts 2 (from the River Lune) and 4 are similar in terms of central tendency and spread, with the same median (28 mm) and standard deviation (12 mm). However, cast 2 is composed of mature fluvial particles that are better rounded than those of cast 4 (Figure 1). This is apparent in a visual classification according to Krumbein's (1941) scheme (Wadell roundness values of 0.8 and 0.5 respectively) and also in mean values of the Dobkins and Folk (1970) roundness index for samples of 100 cast particles: 0.34 and 0.28, respectively, a significant difference (t-test, $\alpha = 0.05$). The contrasts in roughness scale (cast 3 versus 4) and surface smoothness (cast 2 versus 4) that these surfaces exhibit provide a means of exploring the impact (if any) of these two parameters on interfacial flows. Based on two examples, this exploration cannot be exhaustive, but it is nevertheless instructive.

Flume setup and flow conditions

Each cast in turn was positioned in a 9.0 m long, 0.9 m wide, and 0.8 m deep flume with a fixed slope of 0.002. A rhomboidal arrangement of concrete hemispheres (0.08 m diameter, 44 per square meter), placed along the first 6.0 m and the final 1.0 m of the bed, was used to establish a fully-turbulent boundary layer. A cast was positioned between 6.0 and 8.0 m so that its upstream and downstream edges were flush with the boards on which the roughness hemispheres were mounted. The resulting flows were steady, uniform, fully turbulent, and subcritical.

Measurements were made above each of the three casts at three discharges (Q = 0.15, 0.20 and 0.26 $m^3 s^{-1}$) that were set using pump speed and constrained by the abilities of the flume in which the work was conducted. Corresponding flow depths measured to the lowest point on each cast (H), Reynolds numbers (Re), cross-sectional mean velocities (C) and relative submergence (H/Δ where $\Delta = z_{max} - z_{min}$ is roughness height, and z_{max}, z_{min} are the highest and lowest points on the boundary surface, respectively) are given in Table I. For each one of these discharges, water depth (H) was contrived to be almost identical, no matter which cast was present in the flume, by making slight adjustments in the aperture of the undershot tailgate weir. In this regard our experiments are similar to those of Hardy *et al.* (2010) who kept flow depth constant above the three surfaces they examined under two different flow velocities. Here, H varied by only small amounts between casts (maximums of 2, 4 and 5 mm or 0.35, 0.86 and 1.30% of mean H for flows 1, 2, and 3 respectively). Differences in relative submergence (H/Δ) between casts under a given discharge therefore reflect differences in cast roughness height, not water depth (Table I). Observed differences in interfacial measurements between casts can therefore be securely assigned to differences in microtopography, including its effect on relative submergence. At the highest discharge (flow 3), water depths were lowest, so H/Δ decreased as discharge increased above each cast with average values of 6.8, 5.6 and 4.6 for flows 1, 2 and 3 respectively. The effect of changing discharge is therefore manifest as small differences in relative submergence as well as in mean velocity and Reynolds number.

Although relative submergence differs between the nine combinations of flow and cast, H/Δ values have a small range with a mean of 5.7 and standard deviation of 1.3. This positions these flows around the Type II – Type III boundary according to the flow type classification of Nikora *et al.* (2001, 2004) wherein Type IV flows have roughness elements that break the water surface so the interfacial sublayer extends throughout the flow ($H/\Delta < 1.0$); Type III flows ($1.0 < H/\Delta \approx < 5.0$) have a form-induced sublayer that extends to the free surface; deeper, Type II flows are characterised by the addition of a logarithmic velocity layer as the roughness elements are drowned out ($H/\Delta \approx > 5.0$); and Type I flows are further differentiated by the presence of an additional outer layer, at $H >> \Delta$, where viscous effects and form-induced fluxes are negligible. Variations in $H\Delta$ between the nine runs reported here are of interest without being extreme and in all cases reflect conditions in relatively shallow, upland gravel-bed rivers.

Hydraulic measurements

For each patch, the 0.8 × 0.5 m sub-area area was located 0.75 m from the upstream edge of the cast, ensuring that flow in the near-bed region was conditioned by passage over the gravel facsimile and not adversely affected by the transition from hemisphere configuration to cast surface. Velocity time series were sampled using an acoustic Doppler velocimeter (ADV) deployed at 99 locations in an 11 × 9, $x - y$, grid with spacing of 0.1 m and 0.05 m, respectively. At each location, time series were collected at three local heights (0.008, 0.015, 0.030 m) yielding data for three convolute layers (layers a, b and c respectively) that followed the local bed topography. The chosen displacements of these layers ensured that the majority of sampled points were below the highest bed elevations and therefore within the interfacial layer between the grain roughness troughs and crests. Data from any of layers a, b or c that were collected above z_{max}, were excluded from the analysis reported here. The total numbers of data measurement points within the interfacial layer varied between casts and flow combinations, because censoring of ADV data removed more data points from the higher flows and because of differences in cast microtopography, but in all cases the number of interfacial measurements is large, ranging from 231 to 287 locations (Table II).

At each measurement point, instantaneous velocities were measured for the three orthogonal velocity components over a period of 60 s at a sampling frequency of 25 Hz. This combination of sampling frequency and period constitutes an optimal sampling scheme for the ADV (Buffin-Bélanger and Roy, 2005). If used incautiously, ADV measurements are prone to errors (Lane *et al.*, 1998; Nikora and Goring, 1998; Finelli *et al.*, 1999; McLelland and Nicholas, 2000) and a rigorous validation scheme was therefore adopted to filter spurious measurements (Buffin-Belanger *et al.*, 2006).

For each sampling location, mean streamwise velocity, $\overline{u}$ ($m s^{-1}$), and turbulent kinetic energy, K ($J m^{-3}$), were extracted from the velocity time-series, with K calculated as

$$K = 0.5\rho\left(u_{RMS}{}^2 + v_{RMS}{}^2 + w_{RMS}{}^2\right) \quad (1)$$

Table I. Flow characteristics. Q is measured discharge, Re is Reynolds number calculated using the median flow depth above the cast surface, C is average cross-section velocity also estimated using median flow depth above the cast surface, H is maximum water depth (measured from the water surface to the lowest trough on the cast surface) and Δ is roughness height (elevation difference between the lowest and highest points on the cast surface $z_{max} - z_{min}$)

	Flow 1			Flow 2			Flow 3		
Cast	2	3	4	2	3	4	2	3	4
Q ($m^3 s^{-1}$)	0.15	0.15	0.15	0.20	0.20	0.20	0.26	0.26	0.26
C ($m s^{-1}$)	0.310	0.318	0.309	0.511	0.524	0.514	0.814	0.841	0.802
Re	165508	165508	165508	220677	220677	220677	286881	286881	286881
H (m)	0.566	0.566	0.568	0.463	0.465	0.461	0.383	0.385	0.388
Δ(m)	0.070	0.109	0.080	0.070	0.109	0.080	0.070	0.109	0.080
H/Δ	8.1	5.2	7.1	6.6	4.3	5.8	5.5	3.5	4.9

Table II. Number of hydraulic measurement points below the level of cast high points (z_{max}) and therefore within the interfacial layer. Numbers change between flows, despite a common sampling grid above each cast, because quality control of ADV data removed different points and numbers of points at different flows. Numbers change between casts because of differences in microtopography

	Flow 1			Flow 2			Flow 3		
Cast	2	3	4	2	3	4	2	3	4
Number of interfacial time series	263	277	276	268	278	287	253	253	231

where RMS denotes the root-mean square of the velocity time series, u, v and w refer to the streamwise, vertical and cross-stream velocity components and ρ is water density (=1000 kg m^{-3}).

Quadrant analysis was used to investigate the nature of flow motions in the near- bed region and is based on the joint distribution of the velocity fluctuations u' and v' from the mean streamwise and vertical components (Lu and Willmarth, 1973) : $u' = u - \overline{u}$ and $v' = v - \overline{v}$, where u and v are instantaneous velocities and $\overline{u}$ and $\overline{v}$ are mean velocities. Quadrants 2 and 4 have been associated with ejection- and sweep-like flow motions, respectively, and thence with sediment entrainment in rivers (Drake *et al.*, 1988; Nelson *et al.*, 1995; Dey *et al.*, 2011; Keshavarzi *et al.*, 2012). In this analysis, a magnitude threshold or "hole" size of zero was selected when computing the proportion of time spent in each quadrant. The Pearson correlation coefficient r was also computed to quantify the intensity of the relationship between the velocity fluctuations u' and v'.

Autocorrelation functions were computed for each u velocity time series in order to document structural coherence. The time scale (*TS*, s) and the integral time scale (*ITS*, s) extracted from the autocorrelation function, represent a measure of the length of time during which the velocity signals exhibit significant positive autocorrelation and the area under the autocorrelation curve, respectively. Both measures relate to the structural coherence of the signal by giving information on the averaged flow structure: *TSu* provides information about the duration, while *ITSu* provides a measure of the duration weighted by the correlation values. *TSu* and *ITSu* were computed from:

$$TSu = \sum_{t=0}^{t=T} 1/f \tag{2}$$

$$ITSu = \int_{t=0}^{t=T} r_{xx}(t)dt \tag{3}$$

where f is the sampling frequency, $r_{xx}(t)$ is the autocorrelation coefficient between two u-series velocity measurements for a time lag t and T is the time lag where $r_{xx}(t)$ is no longer significantly different from zero.

Statistical analysis

To investigate microtopographic effects on hydraulic parameters, the chosen approach was to statistically test for between-cast differences in the within-cast (that is, spatial) median and variance of all variables extracted from the time series. This was done for data lumped together from all measurement layers (that is, for the whole interfacial data set). As a result, small differences are identifiable because of the large number of measurements within each group. Medians, rather than means, were compared between the three cases, using non-parametric Kruskal–Wallis tests, because non-normality was common in the data sets, including the spatial distributions of quadrant percentages (Kolmogorov–Smirnov tests, $263 < n < 277$, $\alpha = 0.05$), and variances were unequal. For comparison of the spatial variability between the three casts, the Levene test of variance was used. For the same reasons, comparison of central tendency for casts 2 and 4 (difference in particle roundness) and casts 3 and 4 (difference in elevation distribution) were completed using non-parametric Mann–Whitney tests and Levene tests were used to compare spatial variances. We investigated differences between pairs of casts (2 vs 4 and 3 vs 4) only in cases where the three-way comparison recorded a significant result. Using this hypothesis-testing approach, the emphasis is put on documenting subtle but significant differences in the temporal and spatially averaged characteristics of hydraulics within the interfacial layer.

Results

Time-averaged streamwise velocity $\overline{u}$

Across the three casts, individual measurements of time-averaged streamwise velocity $\overline{u}$ varied between −0.03 and 0.25 m s^{-1} (flow 1, Figure 2), –0.05 and 0.43 m s^{-1} (flow 2) and −0.11 and 0.76 m s^{-1} (flow 3). Within-cast (i.e. spatial) median values, $\overline{u}_{50}$ and the corresponding standard deviations $\sigma_{\overline{u}}$ are presented in Table III(a) for each cast. Within the interfacial layer $\overline{u}_{50}$ did not vary significantly between casts for any of the three flows (Table IV; Figure 3). However, there were strong between-cast differences in the spatial variability of $\overline{u}$ across the three surfaces. Levene tests revealed that interfacial layer variance $\sigma_{\overline{u}}^2$ was significantly different between casts at all three flows (Table V). This result was investigated further, by examining differences in the variance of $\sigma_{\overline{u}}^2$ between casts 2 and 4, which have contrasting particle roundness characteristics, and between casts 3 and 4, which differ in elevation distribution. There were significant differences in variance between casts 3 and 4 at all flows, but not between casts 2 and 4 at any flow (Table V). The spatial variability of $\overline{u}$ was consistently highest above cast 3, which is the surface with a broad range of elevations.

Turbulent kinetic energy

Across the three casts, K ranged between 0.2 and 3.2 J m^{-3} (flow 1), 0.53 and 8.71 J m^{-3} (flow 2) and 1.9 and 23.0 J m^{-3} (flow 3). Within-cast (spatial) median values, K_{50} and the corresponding standard deviations, σ_K are presented in Table III(a). Differences in cast microtopography had a strong effect on median turbulent kinetic energy in the interfacial layer with a significant between-cast difference in K_{50} under all three flows (Table IV; Figure 4). Further comparisons of K_{50} between pairs of casts found a significant difference between casts 2 and 4 (contrasting roundness) at flows 1 and 2, and between casts 3 and 4 (which differ in elevation distribution) at flow 3 (Table IV). The impact of surface microtopography on the spatial variability of at-a-point TKE was also assessed. Levene tests revealed that σ_K^2 was not significantly different between the three casts at any flow (Table V).

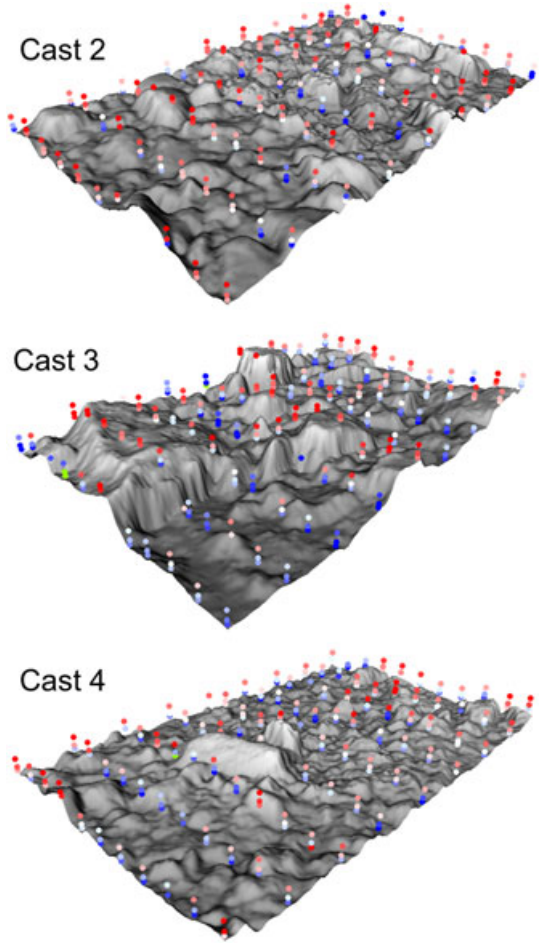

Figure 2. Scatter plot of mean streamwise velocity measurements $\overline{u}$ in the interfacial layer above casts 2, 3 and 4 under flow 1 ($Re = 165508$). A common colour scale is used in which the darkest blue represents $\overline{u} = 0\,m\,s^{-1}$ white represents median velocities in the range $0.135 < \overline{u} < 0.145\,m\,s^{-1}$ and the deepest red represents velocities at the observed maximum of $0.250\,m\,s^{-1}$. Negative velocities appear as green. Blue data points therefore represent below median values and pinks and reds represent above median values.

Quadrant analysis

Across the three casts and flows, the median percentage of time within each quadrant ($Q1_{50}$, $Q2_{50}$, $Q3_{50}$ and $Q4_{50}$) averaged 16.2, 33.6, 17.3 and 32.5%, respectively, and the spatial variance of these proportions across each surface (i.e. between individual locations) was typically 3 to 5% (Figure 5; Table III(b)). It is clear from Figure 5 that differences in quadrant proportions between casts are small at any given flow. Ejection (Q2) and sweep (Q4) events dominate within the interfacial layers above each surface at all three flows, with Q2 having slightly higher proportions in every case

Comparing median time percentages between casts reveals that despite the apparent similarity of the quadrant time distributions, cast microtopography does have a significant effect. This is especially true at flows 1 and 2: $Q1_{50}$, $Q2_{50}$, and $Q3_{50}$ were significantly different between casts at both flows and $Q4_{50}$ was different at flow 2 (Table IV). At flow 3, only the proportion of time in Q2 showed a difference between casts. Additional comparisons of $Q1_{50}$, $Q2_{50}$, $Q3_{50}$ and $Q4_{50}$ between pairs of casts revealed almost no significant differences between casts 2 and 4, which differ in particle roundness, but significant differences for most quadrant time proportions between casts 3 and 4, especially at flows 1 and 2. The surface with less elevation range cast 4 (smaller grain sizes, better sorted) exhibited a significantly greater proportion of ejection and sweep-like events than the 'rougher' cast 3, especially at flows 1 and 2. At flow 3 the magnitude of the differences in mean time proportions between casts 3 and 4 were similar to those for flows 1 and 2 (Table III(b)), but the variance of those proportions was greater (Table III(b)) suggesting that the lack of a significant result at the highest flow reflects an increase in the variability of quadrant time proportions.

While the quadrant analysis provides time proportions, the Pearson correlation coefficient (Table III(b)) provides a measure of the intensity of the linear adjustment between u' and v' and therefore reflects the consistency of the joint velocity fluctuations. Cast microtopography had an effect on this relation at flows 1 and 2 with a significant between-cast difference in the median values, r_{50} within the interfacial layer (Table IV). At flow 3, there was no cast effect on r_{50}. Further comparisons of r_{50} between pairs of casts using Mann–Whitney found no significant differences between casts 2 and 4, which differ in particle roundness, but a significant difference at flows 1 and 2 between casts 3 and 4, which differ in elevation distribution (Table IV). In particular, the coefficients for cast 4 were significantly greater than the coefficients for the rougher cast 3. These results are consistent with the higher combined proportion of time in Q2 and Q4 on cast 4 (at flows 1 and 2), reported above.

The spatial variance of at-a-point quadrant time percentages and of r were not significantly different between casts (Table V) but the observed variances did tend to increase as Re increased (Table III(b)).

Integral time scale

Across the three casts and flows, the median values for within-cast time scale and integral time scale estimates ranged from 0.6 to 1.8 s and from 0.19 to 0.50 s, respectively (Table III(c)). The microtopography of the casts influenced the streamwise coherence of the signal at all three flows, with significant differences in both $ITSu_{50}$ and TSu_{50} between the casts (Table IV). Paired tests revealed that these results originated primarily from differences between casts 3 and 4 (Table IV), with significantly less coherency and shorter periods of coherent flow above the surface that has a greater elevation range (cast 3; Table III(c)).

Surface microtopography had a significant effect on the spatial variability of $ITSu$ and TSu at flow 3, but not at flow 1 (Table V). Paired Levene tests suggest that the difference in σ^2_{ITSu} and σ^2_{TSu} at flow 3 is due to differences between casts 2 and 4 (Table V), with greater spatial variability in structure duration and coherence above the rounded surface of cast 2 and less above the angular surface of cast 4 (Table III(c)).

Discussion

The results of the statistical hypothesis testing can be summarized as follows: (1) differences in grain-scale bed microtopography had no effect on the spatial median of the streamwise mean velocities, $\overline{u}_{50}$, within the interfacial layer, but the spatial variance of $\overline{u}$ was strongly dependent on microtopography; in contrast, (2) differences in grain-scale microtopography did significantly affect median turbulent kinetic energy, K_{50}, but did not affect the spatial variance of K. (3) These results were consistent across all three flows; that is interfacial, mean streamwise velocity and TKE characteristics responded (or not) to microtopographic differences in the same way, irrespective of flow strength. Analyses of flow structures within the interfacial layer indicated that: (4) although sweep and ejection events dominated the interfacial region above all surfaces there was a microtopography effect

Table III. Spatial statistics (mean < >, median and standard deviation) within the interfacial layer above each surface for each flow

	Flow 1			Flow 2			Flow 3		
Cast	2	3	4	2	3	4	2	3	4
(a) Streamwise velocity $\overline{u}$ ($m\,s^{-1}$) (temporal averages over 60 s at 25 Hz) and turbulent kinetic energy K ($J\,m^{-3}$)									
$<\overline{u}>$ ($m\,s^{-1}$)	0.135	0.125	0.133	0.213	0.211	0.223	0.403	0.386	0.402
$\overline{u}_{50}$ ($m\,s^{-1}$)	0.145	0.126	0.140	0.226	0.217	0.233	0.426	0.404	0.413
$\sigma_{\overline{u}}$ ($m\,s^{-1}$)	0.056	0.059	0.050	0.078	0.101	0.075	0.132	0.179	0.129
$<K>$ ($J\,m^{-3}$)	1.427	1.318	1.289	3.029	3.261	3.229	8.858	9.328	8.810
K_{50} ($J\,m^{-3}$)	1.412	1.313	1.264	2.957	3.192	3.081	8.297	9.059	8.327
σ_K ($J\,m^{-3}$)	0.463	0.396	0.450	0.888	0.924	1.126	2.499	2.646	2.649
(b) Proportion of time within each quadrant (%) and the Pearson correlation coefficient of $u'v'$ (60 s time series at 25 Hz)									
$Q1_{50}$ (%)	16.2	17.4	16.5	16.0	16.5	15.5	15.9	16.5	15.7
$Q2_{50}$ (%)	33.9	32.7	33.5	34.3	32.8	33.9	34.2	33.0	34.1
$Q3_{50}$ (%)	17.5	18.0	17.3	17.1	17.8	16.8	16.9	17.3	16.7
$Q4_{50}$ (%)	32.0	31.7	32.5	32.6	32.1	33.4	32.8	33.1	32.7
σ_{Q1} (%)	3.8	3.3	3.4	4.2	3.9	3.7	4.4	3.9	4.9
σ_{Q2} (%)	3.8	3.2	3.4	4.1	3.7	3.9	4.2	3.6	5.1
σ_{Q3} (%)	3.3	2.9	3.3	3.8	3.3	3.7	3.9	3.4	5.0
σ_{Q4} (%)	3.5	3.3	3.7	4.1	3.9	3.8	4.4	4.1	5.2
r_{50}	0.461	0.418	0.463	0.476	0.440	0.485	0.487	0.461	0.494
σ_r	0.177	0.151	0.158	0.204	0.179	0.184	0.200	0.171	0.235
(c) Time scale and integral time scale from the autocorrelation function for the streamwise velocity components (in seconds)									
$<TSu>$ (s)	1.8	1.7	2.1	1.2	1.1	1.3	1.2	0.9	1.1
TSu_{50} (s)	1.5	1.4	1.8	1.0	1.0	1.1	0.8	0.6	0.8
σ_{TSu} (s)	1.1	1.1	1.3	0.8	0.7	0.9	1.3	0.8	0.9
$<ITSu>$ (s)	0.51	0.46	0.54	0.34	0.30	0.35	0.27	0.22	0.25
$ITSu_{50}$ (s)	0.47	0.42	0.50	0.32	0.29	0.33	0.21	0.19	0.22
σ_{ITSu} (s)	0.22	0.20	0.25	0.15	0.11	0.15	0.19	0.11	0.13

Table IV. For each flow, comparison of spatially averaged (median) (i) streamwise velocity $\overline{u}_{50}$ ($m\,s^{-1}$) (ii) turbulent kinetic energy K_{50} ($J\,m^{-3}$), (iii)–(vi) percentage of time in $u'v'$ quadrants $Q1_{50}$, $Q2_{50}$, $Q3_{50}$, and $Q4_{50}$ (vii) $u'v'$ correlation coefficient r_{50}, (viii) streamwise integral time scale $ITSu_{50}$, and (ix) time scale TSu_{50} between casts 2 3 and 4 and between pairs of casts (in cases where the three-way comparison indicates a significant effect): 3 vs 4 for differences in elevation distribution; 2 vs 4 for differences in particle roundness. K-W indicates Kruskall–Wallace test and M-W is Mann–Whitney test

	K-W P-value All casts			M-W P-value 3 vs 4			M-W P-value 2 vs 4		
Flow	1	2	3	1	2	3	1	2	3
$\overline{u}_{50}$	0.090	0.441	0.752	--	--	--	--	--	--
K_{50}	<0.001*	0.003*	0.011*	0.169	0.124	0.009*	<0.001*	0.048*	0.885
$Q1_{50}$	<0.001*	0.004*	0.245	<0.001*	0.001*	--	0.812	0.492	--
$Q2_{50}$	<0.001*	<0.001*	0.008*	<0.001*	<0.001*	0.016*	0.394	0.562	0.618
$Q3_{50}$	0.007*	0.002*	0.587	0.002*	0.001*	--	0.316	0.211	--
$Q4_{50}$	0.058	0.006*	0.879	--	0.003*	--	--	0.015*	--
r_{50}	0.001*	0.005*	0.482	<0.001*	0.002*	--	0.540	0.183	--
$ITSu_{50}$	<0.001*	<0.001*	0.001*	<0.001*	<0.001*	0.001*	0.094	0.078	0.560
TSu_{50}	<0.001*	0.001*	0.003*	<0.001*	<0.001*	0.003*	0.002*	0.141	0.990

*Significant difference at $\alpha = 0.05$.

on quadrant time proportions – specifically slightly (but significantly) lower proportions of ejection and sweep (Q2 and Q4) events above the surface of cast 3, which has the greatest elevation range; that (5) this effect weakened as flow increased, primarily because of an increase in the spatial variability of quadrant time proportions at higher flows; consistent with this, (6) there were significant differences in the strength of Pearson correlations of $u'v'$ between casts which differed in their elevation distributions, but only at flows 1 and 2, so again the topographic effect on r weakened as flow increased; (7) at all flows, microtopography affected the time coherency of flow structures in the interfacial layer (TSu_{50} and $ITSu_{50}$) with differences in elevation distribution (between casts 3 and 4) particularly important; and finally (8) microtopography had no effect on the spatial variability of any of the flow structure parameters examined, except for σ^2_{ITSu} and σ^2_{TSu} at the highest flow.

No measureable impact of microtopography on $\overline{u}_{50}$

The absence of a measureable difference in interfacial $\overline{u}_{50}$ between casts at all three flows suggests that the 'average' interfacial flow velocity may be relatively insensitive to microtopographic roughness across the range of Reynolds numbers examined. This is consistent with field observations of boundary layer flows (Lamarre and Roy, 2005; Legleiter

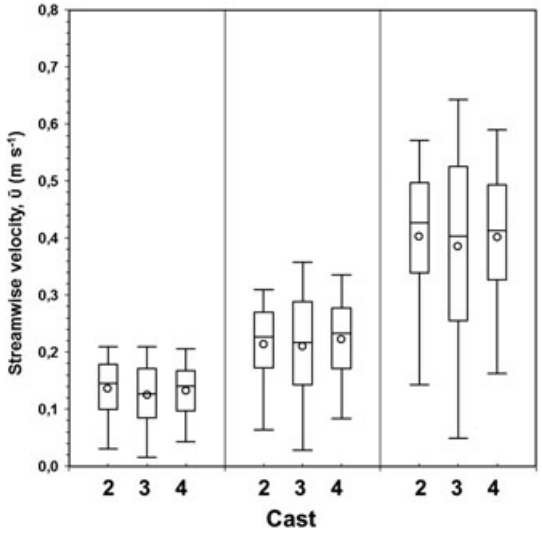

Figure 3. Between-cast variations in time-averaged streamwise velocity $\bar{u}$ ($m\,s^{-1}$) for the interfacial layer at flows 1 (left panel), 2 (middle panel) and 3 (right panel). In each panel, box plots are for 263, 277, and 276 spatially distributed time series (each 60 s at 25 Hz) on casts 2, 3 and 4, respectively. Box plots show 5th and 95th percentiles as whiskers, 25th and 75th percentiles as box ends, the median ($\bar{u}_{50}$) as a solid line and the mean as an open circle.

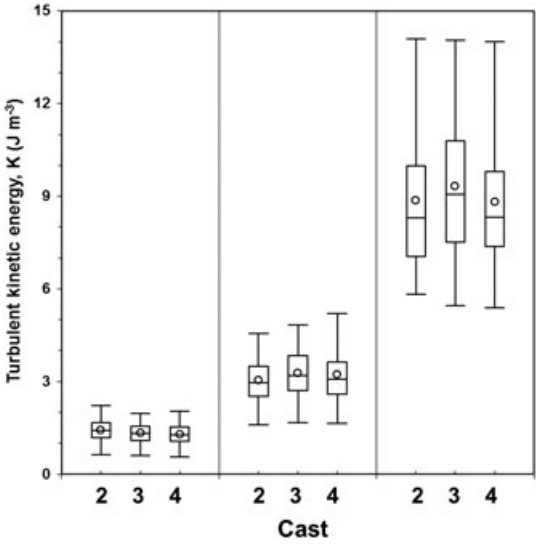

Figure 4. Between-cast variations in turbulent kinetic energy K ($J\,m^{-3}$) for the interfacial layer at flows 1 (left panel), 2 (middle panel) and 3 (right panel). In each panel, box plots are for 263, 277 and 276 spatially distributed time series (each 60 s at 25 Hz) on casts 2, 3 and 4, respectively. Box plots show 5th and 95th percentiles as whiskers, 25th and 75th percentiles as box ends, the median (K_{50}) as a solid line, and the mean as an open circle.

et al., 2007) and laboratory measurements of near-bed flows (Cooper and Tait, 2008), which found that flow depth (relative submergence) was a greater control on streamwise velocities than local microtopography. In contrast, Sambrook Smith and Nicholas (2005) reported a net increase in mean downstream velocity as bed roughness was smoothed out by infilling troughs, but bearing in mind the two-dimensional nature of the surface they examined, their detailed results support our general observation that interfacial velocities are relatively insensitive to microtopographic change. In particular, the increase in streamwise velocity they observed was not spatially uniform and 43% of 280 vertical profiles extracted from their PIV measurements did not change as roughness was reduced (Sambrook Smith and Nicholas, 2005). Only where smoothing almost eliminated topographic variability did the streamwise velocity close to the boundary increase (their Figures 3 and 5) and they observed that positions where infilling had this effect were restricted to locations where smoothing doubled the distance between protruding roughness elements. This highlights the importance of the spacing of key roughness elements as well as their effective height for determining interfacial flow conditions (Nowell and Church, 1979). Hardy *et al.* (2010) noted that smoothing of bed roughness led to a reduction in the magnitude of negative velocities in flow separation zones downstream of protruding elements, but also a growth in the spatial extent of persistent recirculations because of the greater available space for uninterrupted structures to develop. The net effect of smoothing on the spatially averaged interfacial velocity must therefore reflect the spacing and density of key roughness elements, which will also be important controls on the acceleration of flow within preferential flow paths.

Papanicolaou *et al.* (2001) suggest that time-averaged flow characteristics are inadequate for describing the effects of roughness on flow above the roughness tops and our result extends their assertion to include flow in the interfacial layer. The lack of difference between casts 3 and 4 is of particular interest because the surface elevation distributions of casts 3 and 4 have substantially different standard deviations ($\sigma_h = 23$ and 12 mm, respectively) and it has been suggested that σ_h is a hydraulically meaningful measure of bed roughness, at least

Table V. For each flow, comparison of spatial variance of (i) streamwise velocity $\sigma_{\bar{u}}^2$ and (ii) turbulent kinetic energy σ_K^2, (iii)–(vi) percentage of time in $u'v'$ quadrants σ_{Q1}^2, σ_{Q2}^2, σ_{Q3}^2 and σ_{Q4}^2, (vii) $u'v'$ correlation coefficient σ_r^2, (viii) streamwise integral time scale σ_{ITSu}^2, and (ix) time scale σ_{TSu}^2 between all casts and between pairs of casts (in cases where the three-way comparison indicates a significant effect): 3 vs 4 for differences in elevation distribution; 2 vs 4 for differences in particle roundness

	Levene *P*-value All casts			Levene *P*-value 3 vs 4			Levene *P*-value 2 vs 4		
Flow	1	2	3	1	2	3	1	2	3
$\sigma_{\bar{u}}^2$	0.007*	<0.001*	<0.001*	0.001*	<0.001*	<0.001*	0.072	0.690	0.664
σ_K^2	0.224	0.145	0.457	--	--	--	--	--	--
σ_{Q1}^2	0.170	0.066	0.879	--	--	--	--	--	--
σ_{Q2}^2	0.138	0.757	0.367	--	--	--	--	--	--
σ_{Q3}^2	0.558	0.606	0.622	--	--	--	--	--	--
σ_{Q4}^2	0.814	0.239	0.804	--	--	--	--	--	--
σ_r^2	0.323	0.132	0.816	--	--	--	--	--	--
σ_{ITSu}^2	0.099	0.035*	0.001*	--	0.056	0.123	--	0.526	0.023*
σ_{TSu}^2	0.122	0.140	0.001*	--	--	0.245	--	--	0.020*

*Significant difference at $\alpha = 0.05$.

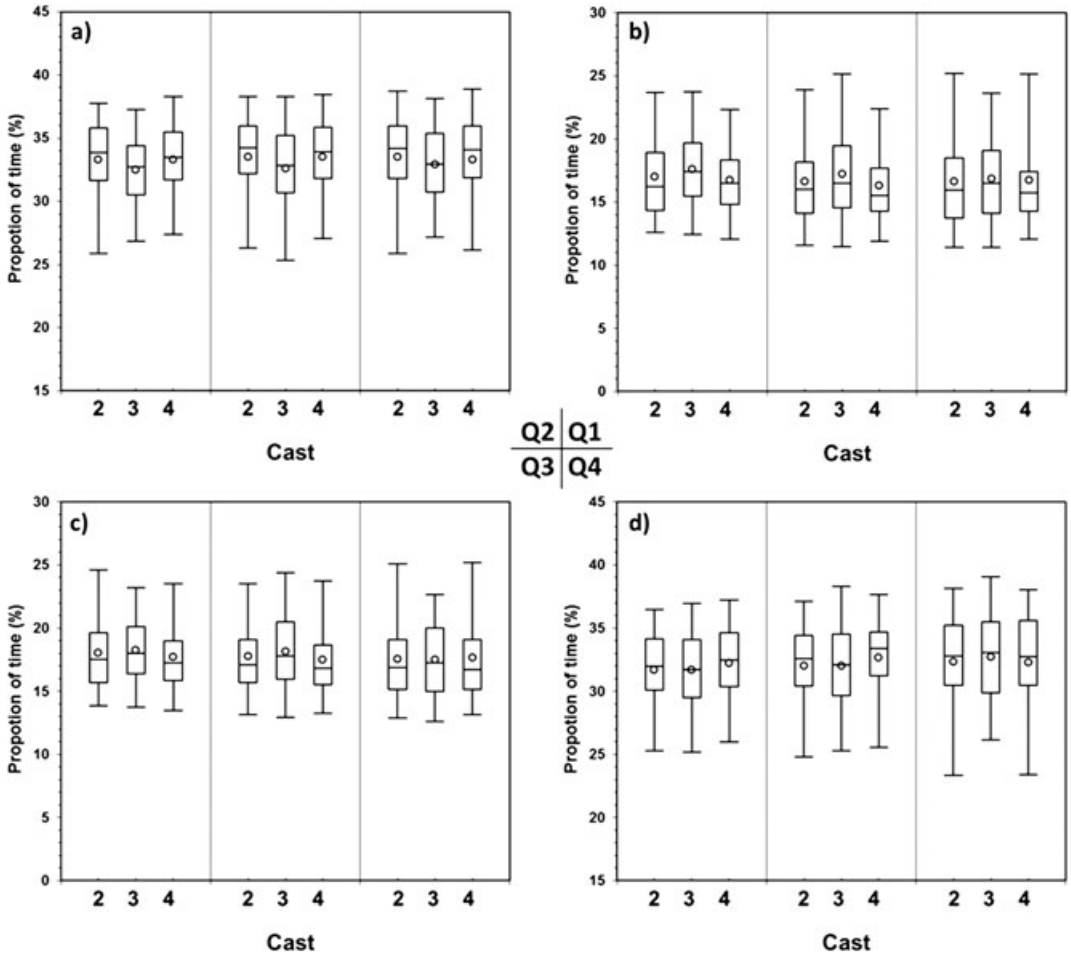

Figure 5. Between-cast comparison of interfacial layer quadrant analysis. Percentage of time observations of the velocity fluctuations u′ and v′ were observed in each quadrant: (a) Q2; (b) Q1; (c) Q3; (d) Q4. In each figure, the left panel is flow 1, middle panel is flow 2 and right panel is flow 3. Box plots are for 263, 277 and 276 spatially distributed time series (each 60 s at 25 Hz) on casts 2, 3 and 4, respectively. Box plots show 5th and 95th percentiles as whiskers, 25th and 75th percentiles as box ends, the median as a solid line, and the mean as an open circle.

for the main body of the flow (Smart *et al.*, 2002; Aberle and Smart, 2003). This result suggests that differences in σ_h do not necessarily translate into differences in interfacial flow characteristics. In turn, it emphasizes the need for continued work to develop measures of surface character and structure that reflect differences in near-bed flow properties (cf. Lane, 2005).

Interfacial and boundary layer velocities

Given the lack of between-cast differences in spatially and temporally averaged interfacial streamwise velocity, it is pertinent to ask whether the apparent differences in cast microtopography are significant in a general context. In particular, it is useful to ask whether the roughness differences between casts might be expected to produce a difference in integral flow properties for the whole boundary layer and specifically, the average cross-section flow velocity estimated using a standard flow resistance equation. If not, then it might be unsurprising to find limited differences in interfacial hydraulics.

A widely utilized resistance formula is one based on Keulegan's integration of the logarithmic law of the wall, such as:

$$C' = \frac{1}{\kappa} \cdot \ln\left(\frac{\alpha d}{z}\right) \cdot (gdS)^{0.5} \tag{4}$$

where C' is predicted mean velocity (m s^{-1}), $\kappa \approx 0.4$ is the von Karman constant, $\alpha = 12.2$ is a cross-sectional-shape factor, d is water depth (m), z is a roughness height (m), $g = 9.81$ is the gravitational acceleration and S is water-surface slope. The roughness height is typically set to some multiple of D_{50} or D_{84} and Ferguson (2007) found $z = 4D_{84}$ to work well for a wide range of gravel-bed rivers characterized by relatively low submergence. It follows from Equation (4) that the absolute difference in estimated velocity for two bed surfaces with different D_{84}, is

$$C'_f - C'_c = 2.5(gdS)^{0.5} \cdot \ln\left(\frac{D_{84c}}{D_{84f}}\right) \tag{5}$$

where subscript c refers to the coarser-grained surface and subscript f to the finer-grained surface. $C'_f - C'_c$ is therefore directly proportional to slope and depth, and also increases with the ratio D_{84c}/D_{84f}. For casts 3 and 4, where $D_{84c}/D_{84f} = 100/61$ mm $= 1.64$, Figure 6 shows differences in estimated velocity for $0.001 \le S \le 0.03$ and $0.20 \le d \le 1.0$ m, which are sensible ranges for upland gravel-bed rivers. Velocity differences range from less than 0.10 m s^{-1} up to 0.6 m s^{-1} and, for our flume setup ($d \approx 0.45$ m and $S = 0.002$), the estimated difference in mean velocity is approximately 0.12 m s^{-1}.

These absolute differences are not trivial and suggest that the differences between casts are significant in a traditional sense; that is, one would expect the change in texture to have an impact on measured velocity in the boundary layer under a range of reasonable flow conditions. In other words, it would be imprudent to ignore microtopographic differences such as these if one were estimating average cross-section velocity

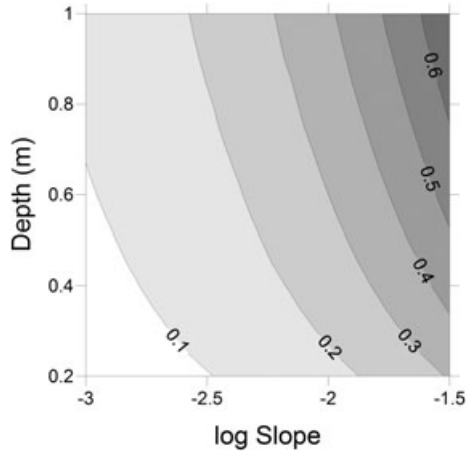

Figure 6. Absolute differences in velocity ($m\,s^{-1}$) estimated using a Keulegan-type approach for surfaces of different D_{84}. Differences are estimated for ranges of slope and depth values that are reasonable for gravel-bed rivers using, as an example, the difference in D_{84} between casts 3 and cast 4.

using a flow resistance equation. This is interesting when set against the finding reported here, that temporally and spatially averaged velocity within the interfacial layer is not significantly affected by these differences in surface microtopography. The comparison suggests that differences in grain roughness sufficient to affect boundary layer flow properties do not necessarily affect mean interfacial velocities.

Gravel-bed microtopography affects $\sigma_{\overline{u}}^2$

At all three flows, the spatial variance of $\overline{u}$ was greatest in the interfacial layer above cast 3, was lower for cast 2 and was lower again for cast 4 (Table III(a)), with significant differences in $\sigma_{\overline{u}}^2$ between casts 3 and 4 in each case (Table V). To further understand the observed significant difference, three-dimensional visualization modelling of the flow parameters was undertaken. An inverse-distance gridding algorithm, with anisotropic search parameters to reflect differences in the orthogonal spacing of data points, was used to interpolate three-dimensional models of $\overline{u}$ (and K) on a 50 by 50 by 50 lattice. Figure 7 shows partly opaque visualizations of three-dimensional renderings of $\overline{u}$ above each cast under flow 1 ($Re = 165508$). Red shades indicate velocities that are above the median (for the flow across all casts), blues indicate below median values and white corresponds to values close to the median. Consistent with the above results, the range and patchiness of shades is greatest above cast 3, less for cast 2 and least for cast 4. Difference in the vertical variability, apparent in the side-on views, are striking: above cast 4 there is a spatially consistent increase in velocity through the depth of the interfacial layer, whereas, above cast 3, and to a lesser extent above cast 2, vertical velocity profiles are less consistent with strong spatial heterogeneity. This is most apparent where flow is accelerated over the cobble-sized clast that cuts the left-hand edge of the measurement area. These images suggest that variance is highest above cast 3 because of the wide distribution of surface elevation with high relief elements generating strong planar velocity gradients (and therefore spatial patchiness) that extend through the full depth of the interfacial layer. This is in contrast to the less rugged surfaces (lower elevation variance), especially cast 4, where there are fewer high-relief elements, there is less blocking, acceleration and recirculation associated with large protuberances and a more consistent pattern of vertical variation throughout the whole layer. Elevation distribution therefore helps to explain the observed difference in velocity variance between the surfaces.

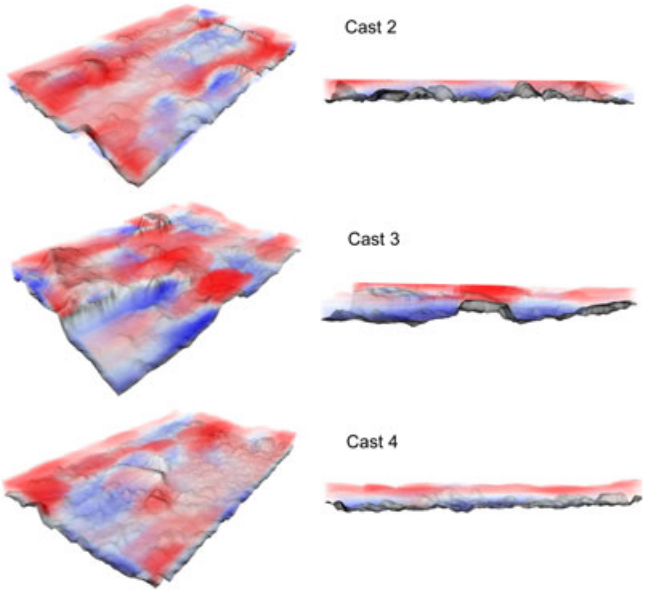

Figure 7. Semi-opaque visualization of interpolated streamwise velocity, $\overline{u}$, under flow 1 ($Re = 165508$) over the three casts in both a perspective view (left-hand column) and looking in from the left-hand edge of the flow measurement volume (right-hand column). Flow is from top right to bottom left and from right to left, respectively. Red shades indicate velocities that are above the median (for the entire data set), blues indicate below median values and white corresponds to values close to the median.

These visualizations are consistent with planar visualizations of velocity variations extracted from numerical models of near-bed flows (Hardy *et al.*, 2007) and, although they do not comment on it directly, these results are also consistent with data presented by Sambrook Smith and Nicholas (2005) and Hardy *et al.* (2010) in which increased microtopographic relief is associated with greater spatial variability of interfacial velocities (their Figure 2 and Figure 3, respectively).

Gravel-bed microtopography affects K_{50}

Pair-wise comparisons designed to investigate the impact of elevation distribution and particle roundness on observed hydraulics, suggest that the significant between-cast differences in median turbulent kinetic energy values K_{50} under all three flows, could have been driven by different microtopographic factors, depending on the flow Reynolds number (Figure 4, Table III(a)). Significant differences in K_{50} between casts 2 and 4, at flows 1 and 2, were not observed at flow 3, while a significant difference between casts 3 and 4 at flow 3, was not repeated at flows 1 and 2. This implies that particle roundness had an effect at lower Reynolds numbers but that elevation distribution had an effect only at the highest Reynolds number.

However, examination of Figure 8 suggests that the difference in particle roundness is not the only relevant distinction between casts 2 and 4. Despite the similarity in elevation statistics (e.g. identical median elevations and σ_h), the high elevations on cast 4 are associated with a single coarse cluster in the centre right of the patch. This is in contrast to cast 2, where the upper tail of the elevation distribution is associated with a larger number of spatially distributed clasts. Previous observations of near-bed turbulence have found that maximum values of K or other measures of turbulence intensity are associated with shedding vortices downstream of large roughness elements (Nowell and Church, 1979; Buffin-Belanger *et al.*, 2006; Mignot *et al.*, 2009; Hardy *et al.*, 2009). In the case of cast 2, the spatial distribution of these roughness elements

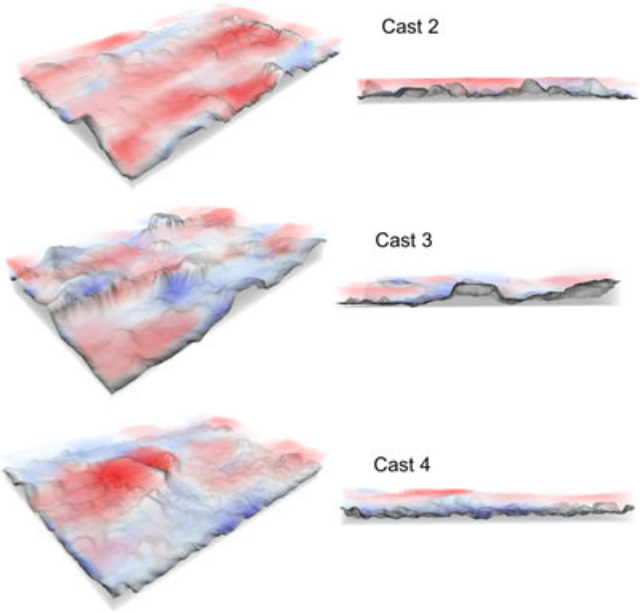

Figure 8. Semi-opaque visualisation of interpolated turbulent kinetic energy, *K*, under flow 1 (*Re* = 165508) over the three casts in both a perspective view (left-hand column) and looking in from the left-hand edge of the flow measurement volume (right-hand column). Flow is from top right to bottom left and from right to left, respectively. Red shades indicate turbulent kinetic energies that are above the median (for the entire data set), blues indicate below median values and white corresponds to values close to the median.

ensures widespread generation of such vortices and a high average value of K_{50} in the interfacial layer. In contrast, the single large protuberance on cast 4 has a local effect that does not unduly weight K_{50} (Figure 8).

The difference in K_{50} between casts 2 and 4 at flows 1 and 2 may not, therefore, be due to a difference in clast roundness but seems more likely to reflect a difference in the spatial arrangement and density of protruding roughness elements. Following Morris's (1955) flow typonomy, Nowell and Church (1979) found maximum turbulence intensity was associated with wake-interaction flows produced by moderate densities of distributed roughness elements. In contrast with the isolated roughness of cast 4, cast 2 is characterized by such a moderate distribution of roughness elements. At flow 3 it is apparent that this distinction becomes less important and instead the difference in elevations between casts 3 and 4 has an effect, with significantly higher median turbulence intensity above the surface of greater relief (cast 3). That the roughness density effect on TKE diminishes with flow is consistent with Hardy *et al.*'s (2009) observation that as Reynolds number increased, wake zones of vortex shedding and intense shear above protruding elements lengthened and merged to form a unified region of heightened turbulence in which microtopographic effects became unimportant. Hardy *et al.* (2010) observed that increasing relief had a similar impact, raising overall levels of turbulence intensity because of the presence of larger patches of more intense vortex shedding. Sambrook Smith and Nicholas (2005) also found higher levels of turbulence above rougher surfaces. These observations provide a possible explanation for the apparent importance of elevation difference at flow 3 in our experiments, suggesting that under the high flow, when the flow was arguably relatively insensitive to roughness element distribution, the elevation differences across cast 3 (compared with those of cast 4) were nevertheless sufficient to generate intense flow separation and produce high values of TKE.

Gravel-bed microtopography affects coherent flow structures

Coherent flow structures were documented using classic quadrant analysis, the Pearson correlation coefficient and the time scales extracted from the autocorrelation function for the streamwise velocity component. For all of these parameters, under two of the three flows, small but significant differences were observed between casts.

For all casts and flows, Q2 and Q4 events dominate the time series, with the proportion of time for Q2 slightly higher than Q4. Ejection- and sweep-like events therefore prevail in the interfacial layer irrespective of *Re*, consistent with numerous earlier observations for near-bed flows above gravelly surfaces (Nelson *et al.*, 1995; Buffin-Belanger and Roy, 1998; Sambrook Smith and Nicholas, 2005; Hardy *et al.*, 2009). Higher proportions of time in Q2 suggest a dominance of slower, upward ejections, which is in contrast to Sarkar and Dey (2010) and Hardy *et al.* (2010) who found that Q4 sweep events contributed most to interfacial Reynolds stresses in the near-bed region. However, in both cases a threshold ('hole') value was used to exclude relatively low magnitude events, so their results imply that of the relatively high magnitude events, sweeps prevail. Combined with our data, which were analysed without applying a threshold, this suggests that Q2 events are more frequent but less intense than Q4 within the interfacial layer. This is consistent with the analysis of Sambrook Smith and Nicholas (2005) who found that below the roughness tops of their surfaces, Q2 events dominated over Q4 events overall, but that when a threshold was applied, Q4 events dominated.

Flow structure parameters were affected by microtopography, with small but significant differences between casts 3 and 4: specifically, there were fewer Q2 and Q4 events and weaker *u'v'* correlations above cast 3 (Table IV). Recall that cast 3 has a greater roughness height compared with casts 2 and 4 (41 versus 28 mm) and a larger spread of elevations ($\sigma_h = 23$ versus 12 mm). This microtopographic effect was dependent on flow – the proportion of time in Q2 was significantly less above cast 3 under all flows, but the other quadrants did not show between-cast differences at flow 3 when *Re* was highest (Table IV). This result suggests that turbulent flows within the interfacial layer were more highly structured (there was a slightly larger proportion of ejection and sweep events) for surfaces with smaller, less variable roughness heights but that this effect weakened (quadrant distributions became more homogeneous) at the highest *Re* (= 286881) such that only ejection events showed a significant difference caused by roughness. Working at lower *Re* (13000 to 25000) and using a threshold value, Hardy *et al.* (2010) noted that a band of intense Q2 activity, which was apparent above each of their surfaces, moved closer to the bed as surface roughness decreased. This is consistent with our observation that Q2 events were more prolific in the interfacial layer over the less rough surfaces. Our results contrast with those of Sambrook Smith and Nicholas (2005) who observed a reduction in high magnitude (above threshold) Q2 and Q4 events, as roughness declined and concluded that for smoother beds, high magnitude quadrant time proportions become more homogeneous. This contrast almost certainly reflects the fact that we did not apply a magnitude filter and suggests that while high magnitude quadrant events may decline in dominance with a reduction in microtopographic relief, the distribution of all events becomes more homogeneous as microtopographic relief increases.

TSu_{50} and $ITSu_{50}$ were significantly smaller above the rough surface of cast 3 under all three flows (Tables III(c) and IV), which indicates that structures have a shorter duration and that there is more important flow mixing above the roughest

surface. In addition, the values of TSu_{50} and $ITSu_{50}$ approximately halve as *Re* increases from 165508 to 286881, between flows 1 and 3. This reveals that the flow structures are of shorter duration and that mixing increases as *Re* increases. These observations are consistent with those above, implying that flow structures are better defined above the less rough surfaces and that they become less persistent at the highest Reynolds number we examined.

In sum, the measured impacts of microtopography on flow structure parameters suggest that more complex microtopography hinders the formation, but more so the development, of coherent flow structures in the interfacial layer and, although this appears to be true across a wide range of *Re*, in very turbulent flows structures become less persistent and the microtopographic effect is less important. Thus, the velocity signature tends towards a more homogeneous quadrant distribution for the flow over the roughest surface (cast 3), where the proportions of Q2 and Q4 events are lowest, the proportions of Q1 and Q3 events are highest, the *u′v′* correlation coefficients are the weakest and structure durations are the shortest, especially under the highest *Re* flow. A general conclusion is that where roughness heights are more diverse and where *Re* is large, flow structures (undifferentiated by magnitude) are on average likely to be slightly (but significantly) less clearly defined and less persistent within the interfacial layer. This may be because there is a greater chance that a structure initiated in the lee of one protruding element is disrupted by another protrusion or by advecting eddies before it can evolve in size and intensity. An important caveat here is that the relative roughness value for cast 3 is consistently the lowest among the three casts for each flow and that H/Δ declined with *Re* in our experiments (Table I). Although H/Δ values indicate that flow types were similar according to Nikora *et al.*'s (2001, 2004) classification, a legitimate possibility is that the significant differences we have noted between casts 3 and 4 are affected by differences in average submergence.

Conclusions

Our results are broadly consistent with those of previous examinations of roughness effects in depth-limited flows, although the analysis presented here is unique in terms of the focus on interfacial hydraulics, spatially averaged 'patch scale' metrics and a statistical approach to data analysis. The three surfaces that we examined do not, of course, constitute a comprehensive representation of those that occur in nature. We cannot therefore, say very much about the universality of our findings; that is, we cannot provide a general argument about the range of roughness and flow conditions across which our results can be assumed to hold. However, the three surfaces examined are characteristic of natural gravel-bed river textures and the ranges of *Re* and relative submergence are representative of depth-limited flows in upland gravel-bed rivers. For each surface and flow, hydraulic data collection was intensive, yielding a very good appreciation of the spatial and temporal variability of flow parameters within the respective interfacial layers. In this context, the following conclusions are possible:

1. For relative submergence values between 3.5 and 8.1, grain-scale bed microtopography affected different flow properties within the interfacial layer in contrasting ways. Differences in surface roughness were associated with significant differences in the spatial variance of time-averaged streamwise velocity $\sigma_{\overline{u}}^2$, but did not affect spatially averaged (median) values of $\overline{u}$. In contrast, most spatially averaged turbulence parameters within the interfacial layer, including median turbulent kinetic energy *K*, and median values for several structure parameters (*Q1* to *Q4, r, TSu, ITSu*) varied significantly between surfaces but, in most cases, their spatial variance was consistent across the different surfaces (compare Tables IV and V). In line with Papanicolaou *et al.*'s (2001) demonstration that in the outer zone turbulent properties are more sensitive to roughness than time-averaged flow properties, our results suggest that within the interfacial layer, spatially averaged turbulence properties are sensitive to patch roughness but spatially averaged mean velocity is not.
2. Whether or not microtopography had an effect on interfacial streamwise velocity and turbulence intensity (TKE) was independent of flow Reynolds number, but the impacts of microtopography on flow structure parameters showed some flow dependency, with a reduction in the effect of roughness at very high *Re*. This result is tentative because although relative roughness values are similar across all experiments, there is a shift toward lower submergence under the highest flow and increased depth limitation may be an uncontrolled factor.
3. From comparisons between pairs of surfaces that differ in particle roundness and elevation distribution there is some evidence that gravel-bed surfaces of higher, more variable relief generate greater spatial variability in interfacial streamwise velocity and generate less clearly defined, less persistent flow structures in the interfacial layer. However, some caution is required here, because the comparisons were made between natural water-lain surfaces where differences in grain roughness might reside in factors other than particle roundness and elevation distribution, for example, in differences in packing arrangements, in bedform occurrence, or simply in the random arrangement of grains and the microtopographic particularities of these specific surfaces. Indeed, it seems likely that the arrangement of large roughness elements rather than particle roundness is a relevant factor for explaining observed differences in turbulence intensity between casts 2 and 4. The comparisons made here cannot be viewed as a definitive test of particle roundness and microtopographic elevation effects, but they have generated new hypotheses that are worthy of further investigation.

A potentially important implication of our observations for hydraulic, sediment transport and ecological modelling across patchy gravel substrates is that for relative submergence values between approximately 3 and 8, differences in surface microtopography do not *necessarily* produce differences in patch-scale spatial statistics (median, variance) within the interfacial layer. The result for median streamwise velocity is particularly interesting: water-lain gravel beds that are of distinctive appearance, characterized by different roughness parameters and with different boundary-layer flow properties for a given discharge, do not *necessarily* generate detectable differences in streamwise velocity within the interfacial layer. This implies that there is not a simple relation between boundary-layer and interfacial-layer flow properties. Therefore, it is not possible to look at two different sediment patches in a gravel-bed river and assume that the interfacial layer hydraulics within those two patches are different (Jowett, 2003). This is important, because interfacial-layer flows dominate the lives of benthic fauna and are central to sediment transport processes. In the absence of direct interfacial measurements, differences in near-bed flow properties are often assumed to exist between contrasting textural patches and implications might then be drawn about how imagined differences in near-bed hydraulics affect substrate ecology or bed sediment movement. For example, it might be supposed that a coarser substrate offers greater hydraulic refuge for benthic fauna because of lower average velocities, but the results herein suggest that such an assumption

may be misplaced. A related problem is that, because interfacial flows are seldom measured in the field, it is sometimes assumed that relations exist between flow properties measured above the bed and those at the bed. Our results suggest that the use of boundary layer flow measurements as surrogates for benthic, interfacial layer information, is highly problematic.

Finally, our observations highlight the need for better parameterization and understanding of grain-scale roughness and flow resistance in gravel-bed rivers. Although several results hint at what aspects of the surface microtopography are actually important for controlling interfacial flow characteristics, understanding of the relevant contributions of elevation distribution, particle roundness, and roughness element density and arrangement remain poorly constrained. Systematic examination of hydraulics across gradients of these microtopographic variables in flume experiments (Sambrook Smith and Nicholas, 2005; Canavaro *et al.*, 2007; Hardy *et al.*, 2010) and using numerical simulations may be valuable. However, notwithstanding numerous recent advances (Hodge *et al.*, 2009; Large and Heritage, 2012; Bertoldi *et al.*, 2012) there is also a continued (cf. Lane, 2005) and parallel need to develop better means of routinely acquiring patch-scale DEMs or other surface representations, from which *suitable* roughness parameterizations are extracted. For example, although there are some exciting recent developments (Papanicolaou *et al.*, 2012) there is no standard, accepted means of identifying and codifying 'large roughness elements' within the microtopographic confusion that characterizes gravel-bed sediment textures, or of describing their arrangement and distribution. This is despite widespread acknowledgment (Morris, 1955, et seq.) supported by plenty of experimental evidence that such roughness elements are important for understanding depth-limited flows and the extraction of energy from flowing water in gravel-bed rivers.

Acknowledgements—The project was funded by NERC Grant NER/B/S/2000/00697 to Rice, Reid and Jill Lancaster. John Laronne, David Graham and Jim Chandler assisted with casting the river bed patches in the field. We are grateful to Natasha Todd-Burley, Mick Barker, David Graham and Stuart Ashby for their help with the flume experiments, which were conducted in the Department of Civil & Building Engineering at Loughborough University. We are also grateful for two thorough, constructive reviews and the advice of the editors which substantially improved the quality of this paper, though any shortcomings remain our own.

References

Aberle J, Smart GM. 2003. The influence of roughness structure on flow resistance in mountain streams. *Journal of Hydraulic Research* **41**: 259–269.

Bertoldi W, Piegay H, Buffin-Bélanger T, Graham D, Rice SP. 2012. Applications of close-range imagery in river research. In Fluvial Remote Sensing for Science and Management, Carbonneau PE, Piegay H (eds). Wiley-Blackwell: Oxford; 341–366.

Bluck BJ. 1987. Bed forms and clast size changes in gravel-bed rivers. In River Channels: Environment and Process, Richards K (ed). Blackwell: Oxford; 159–178.

Brooks AJ, Haeusler T, Reinfelds I, Williams S. 2005. Hydraulic microhabitats and the distribution of macroinvertebrate assemblages in riffles. *Freshwater Biology* **50**: 331–344.

Buffin-Bélanger T. 2001. Structure d'un écoulement turbulent dans un cours d'eau à lit de graviers en présence d'amas de galets. Unpublished PhD thesis, Université de Montréal.

Buffin-Bélanger T, Reid I, Rice S, Chandler J, Lancaster J. 2003. A casting procedure for reproducing coarse-grained sedimentary surfaces. *Earth Surface Processes and Landforms* **28**: 787–796.

Buffin-Bélanger T, Rice SP, Reid I, Lancaster J. 2006. Spatial heterogeneity of near-bed hydraulics above a patch of river gravel. *Water Resources Research* **42**: W04413. doi: 10.1029/2005WR004070.

Buffin-Bélanger T, Roy AG. 1998. Effects of a pebble cluster on the turbulent flow field of a depth-limited flow in a gravel-bed river. *Geomorphology* **25**: 249–267.

Buffin-Bélanger T, Roy AG. 2005. One minute in the life of a river: selecting the optimal record length for the measurement of turbulence in fluvial boundary layers. *Geomorphology* **68**: 77–94.

Canavaro F, Paris E, Solari L. 2007. Effects of macro-scale bed roughness geometry on flow resistance. *Water Resources Research* **43**. doi: 10.1029/2006WR005727.

Casas MA, Lane SN, Hardy RJ, Benito G, Whiting PJ. 2010. Reconstruction of subgrid-scale topographic variability and its effect upon the spatial structure of three-dimensional river flow. *Water Resources Research* **46**. doi: 10.1029/2009WR007756.

Chandler JH, Buffin-Bélanger T, Rice SP, Reid I, Graham DJ. 2003. The accuracy of a river-bed casting system and the effectiveness of an amateur digital camera for recording river bed fabric. *The Photogrammetric Record* **18**: 209–223.

Cleaver J, Yates B. 1976. The effect of reentrainment on particle deposition. *Chemical Engineering Science* **31**: 983–992.

Clifford NJ. 1996. Morphology and stage-dependent flow structure in a gravel-bed river. In Coherent Flow Structures in Open Channels, Ashworth P, Best JL, Bennett SJ, McLelland SJ (eds). John Wiley and Sons: Chichester; 545–566.

Clifford NJ, Hardisty J, French JR, Hart S. 1993. Downstream variation in bed material characteristics: a turbulence controlled form-process feedback mechanism. In Braided Rivers; Geological Society Special Publication no. 75, Best JL, Bristow CS (eds). The Geological Society: London; 89–104.

Clifford NJ, Robert A, Richards KS. 1992. Estimation of flow resistance in gravel-bed rivers: a physical explanation of the multiplier of roughness length. *Earth Surface Processes and Landforms* **17**: 111–126.

Cooper JR. 2012. Does flow variance affect bedload flux when the bed is dominated by grain roughness? *Geomorphology* **141-142**: 160–169.

Cooper JR, Tait SJ. 2008. The spatial organisation of time-averaged streamwise velocity and its correlation with the surface topography of water-worked gravel beds. *Acta Geophysica* **56**: 614–642.

Cooper JR, Tait SJ. 2009. Water-worked gravel beds in laboratory flumes - a natural analogue? *Earth Surface Processes and Landforms* **34**: 384–397.

Crowder DW, Diplas P. 2000. Using two-dimensional hydrodynamic models at scales of ecological importance. *Journal of Hydrology* **230**: 172–191.

Dancey CL, Balakrishnan M, Diplas P, Papanicolaou AN. 2000. The spatial inhomogeneity of turbulence above a fully rough packed bed in open channel flow. *Experiments in Fluids* **29**: 402–410.

Davis JA, Barmuta LA. 1989. An ecologically useful classification of mean and near-bed flows in streams and rivers. *Freshwater Biology* **21**: 271–282.

Dey S, Sarkar S, Solari L. 2011. Near-bed turbulence characteristics at the entrainment threshold of sediment beds. *Journal of Hydraulic Engineering* **137**: 945–958.

Dittrich A, Koll K 1997. Velocity field and resistance of flow over rough surfaces with large and small relative submergence. *International Journal of Sediment Research* **3**: 21–33.

Dobkins JE, Folk RL. 1970. Shape development on Tahiti-Nui. *Journal of Sedimentary Petrology* **40**: 1167–1203.

Drake TG, Shreve RL, Dietrich WE, Whiting PJ, Leopold LB. 1988. Bed load transport of fine gravel observed by motion-picture photography. *Journal of Fluid Mechanics* **192**: 193–217.

Ferguson R. 2007. Flow resistance equations for gravel- and boulder-bed streams. *Water Resources Research* **43**. W05427. doi:10.1029/2006WR005422

Ferreira RML, Ferreira LM, Ricardo AM, Franca MJ. 2010. Impacts of sand transport on flow variables and dissolved oxygen in gravel-bed streams suitable for salmonid spawning. *River Research and Applications* **26**: 414–438.

Finelli CM, Hart DD, Fonseca DM. 1999. Evaluating the spatial resolution of an Acoustic Doppler Velocimeter and the consequences for measuring near-bed flows. *Limnology and Oceanography* **44**: 1793–1801.

Franca MJ, Ferreira RML, Lemmin U. 2008. Parameterization of the logarithmic layer of double-averaged streamwise velocity profiles in gravel-bed river flows. *Advances in Water Resources* **31**: 915–925.

Garcia C, Cohen H, Reid I, Rovira A, Ubeda X, Laronne JB. 2007. Processes of initiation of motion leading to bedload transport in gravel-bed rivers. *Geophysical Research Letters* **33**. doi: 10.1029/2006GL028865.

Grass AJ. 1971. Structural features of turbulent flow over smooth and rough boundaries. *Journal of Fluid Mechanics* **50**: 233–255.

Hardy RJ, Best JL, Lane SN, Carbonneau P. 2009. Coherent flow structures in a depth-limited flow over a gravel surface: the role of near-bed turbulence and influence of Reynolds number. *Journal of Geophysical Research* **114**: F01003.

Hardy RJ, Best JL, Lane SN, Carbonneau P. 2010. Coherent flow structures in a depth-limited flow over a gravel surface: the influence of surface roughness. *Journal of Geophysical Research* **115**: F03006.

Hardy RJ, Lane SN, Ferguson RI, Parsons DR. 2007. Emergence of coherent flow structures over a gravel surface: a numerical experiment. *Water Resources Research* **43**. doi: 10.1029/2006WR004936.

Hodge RA, Brasington J, Richards K. 2009. Analysing laser-scanned digital terrain models of gravel bed surfaces: linking morphology to sediment transport processes and hydraulics. *Sedimentology* **56**: 2024–2043.

Jowett IG. 2003. Hydraulic constraints on habitat suitability for benthic invertebrates in gravel-bed rivers. *River Research and Applications* **19**: 495–507.

Keshavarzi A, Ball J, Nabavi H. 2012. Frequency pattern of turbulent flow and sediment entrainment over ripples using image processing. *Hydrology and Earth System Sciences* **16**: 147–156.

Kirchner JW, Dietrich WE, Iseya F, Ikeda H. 1990. The variability of critical shear stress friction angle and grain protrusion in water-worked sediments. *Sedimentology* **37**: 647–672.

Kirkbride AD. 1993. Observation of the influence of bed roughness on turbulence structure in depth limited flows over gravel beds. In Turbulence: Perspectives on Flow and Sediment Transport, Clifford NJ, French JR, Hardisty J (eds). John Wiley and Sons: Chichester; 185–196.

Krumbein WC. 1941. Measurement and geological significance of shape and roundness of sedimentary particles. *Journal of Sedimentary Research* **11**: 64–72.

Lacey RWJ, Roy AG. 2007. A comparative study of the turbulent flow field with and without a pebble cluster in a gravel bed river. *Water Resources Research* **43**: W03416. doi: 10.1029/2006WR005044.

Lacey RWJ, Roy AG. 2008. The spatial characterization of turbulence around large roughness elements in a gravel-bed river. *Geomorphology* **102**: 542–553.

Lamarre H, Roy AG. 2005. Reach scale variability of turbulent flow characteristics in a gravel-bed river. *Geomorphology* **68**: 95–113.

Lancaster J. 1999. Small scale movements of lotic macroinvertebrates with variations in flow. *Freshwater Biology* **41**: 605–619.

Lane SN. 2005. Roughness: time for a re-evaluation? *Earth Surface Processes and Landforms* **30**: 251–253.

Lane SN, Biron PM, Bradbrook KF, Butler JB, Chandler JH, Crowell MD, McLelland SJ, Richards KS, Roy AG. 1998. Three-dimensional measurement of river channel flow processes using acoustic doppler velocimetry. *Earth Surface Processes and Landforms* **23**: 1247–1267.

Lane SN, Hardy RJ, Ingham DB, Elliott L. 2004. Numerical modelling of flow processes over gravelly-surfaces using structured grids and a numerical porosity treatment. *Water Resources Research* **40**: W01302. doi: 10.1029/2002WR001934.

Large A, Heritage G. 2012. Ground based LiDAR and its application to the characterisation of fluvial forms. In Fluvial Remote Sensing for Science and Management, Carbonneau PE, Piegay H (eds). Wiley-Blackwell: Oxford; 341–366.

Lawless M, Robert A. 2001a. Scales of boundary resistance in coarse-grained channels: turbulent velocity profiles and implications. *Geomorphology* **39**: 221–238.

Lawless M, Robert A. 2001b. Three-dimensional flow structure around small-scale bedforms in a simulated gravel-bed environment. *Earth Surface Processes and Landforms* **26**: 507–522.

Legleiter CJ, Phelps TL, Wohl EE. 2007. Geostatistical analysis of the effects of stage and roughness on reach-scale spatial patterns of velocity and turbulence intensity. *Geomorphology* **83**: 322–345.

Lu SS, Willmarth WW. 1973. Measurements of the structures of the Reynolds stress in a turbulent boundary layer. *Journal of Fluid Mechanics* **60**: 481–511.

Marquis G, Roy AG. 2011. Bridging the gap between turbulence and larger scales of flow motions in rivers. *Earth Surface Processes and Landforms* **36**: 563–568.

McLelland SJ, Nicholas AP. 2000. A new method for evaluating errors in high frequency ADV measurements. *Hydrological Processes* **14**: 351–366.

Mignot E, Barthelemy E, Hurther D. 2009. Double-averaging analysis and local flow characterization of near-bed turbulence in gravel-bed channel flows. *Journal of Fluid Mechanics* **618**: 279–303.

Morris HM. 1955. Flow in rough conduits. *Transactions of the American Society of Civil Engineers* **120**: 373–398.

Nelson JM, Shreve RL, McLean SR, Drake TG. 1995. Role of near bed turbulence structure in bed load transport and bed form mechanics. *Water Resources Research* **31**: 2071–2086.

Nikora VI, Goring DG. 1998. ADV turbulence measurements: can we improve their interpretation? *Journal of Hydraulic Engineering* **124**: 630–634.

Nikora VI, Goring DG, Biggs BJF. 1998. On gravel-bed roughness characterisation. *Water Resources Research* **34**: 517–527.

Nikora VI, Goring D, McEwan I, Griffiths G. 2001. Spatially averaged open-channel flow over rough bed. *Journal of Hydraulic Engineering* **127**: 123–133.

Nikora VI, Koll K, McEwan I, McLean S, Dittrich A. 2004. Velocity distribution in the roughness layer of rough-bed flows. *Journal of Hydraulic Engineering* **130**: 1036–1042.

Nino Y, Garcia MH. 1996. Experiments on particle-turbulence interactions in the near-wall region of an open channel flow: Implications for sediment transport. *Journal of Fluid Mechanics* **326**: 285–319.

Nowell AR, Church M. 1979. Turbulent flow in a depth-limited boundary layer. *Journal of Geophysical Research* **84**: 4816–4824.

Nowell ARM, Jumars PA. 1984. Flumes - theoretical and experimental considerations for simulation of benthic environments. *Oceanography and Marine Biology Annual Review* **25**: 91–112.

Oldmeadow DF, Lancaster J, Rice SP. 2010. Drift and settlement of stream insects in a complex hydraulic environment. *Freshwater Biology* **55**: 1020–1035.

Paiement-Paradis G, Marquis G, Roy AG. 2011. Effects of turbulence on the transport of individual particles as bedload in a gravel-bed river. *Earth Surface Processes and Landforms* **36**: 107–116.

Papanicolaou AN, Diplas P, Dancey CL, Balakrishnan M. 2001. Surface roughness effects in near-bed turbulence: implications to sediment entrainment. *Journal of Engineering Mechanics* **127**: 211–218.

Papanicolaou AN, AG Tsakiris, K Strom. 2012. The use of fractals to quantify the morphology of cluster microform. *Geomorphology* **139-140**: 91–108.

Rice SP, Buffin-Bélanger T, Lancaster J, Reid I. 2008. Movements of a macroinvertebrate (Potamophylax latipennis) across a gravel-bed substrate: effects of local hydraulics and micro-topography under increasing discharge. In Gravel-bed rivers VI: From Process Understanding to River Restoration, Habersack H, Piegay H, Rinaldi M (eds). Elsevier BV: Amsterdam; 637–660.

Robert A. 1988. Statistical properties of sediment bed profiles in alluvial channels. *Mathematical Geology* **29**: 205–223.

Robert A. 1990. Boundary roughness in coarse-grained channels. *Progress in Physical Geography* **14**: 42–70.

Robert A. 1993. Bed configuration and microscale processes in alluvial channels. *Progress in Physical Geography* **17**: 123–136.

Robert A, Roy AG, De Serres B. 1992. Changes in velocity profiles at roughness transition in coarse-grained channels. *Sedimentology* **39**: 725–735.

Roy AG, Buffin-Bélanger T, Lamarre H, Kirkbride AD. 2004. Size shape and dynamics of large-scale turbulent flow structures in a gravel-bed river. *Journal of Fluid Mechanics* **500**: 1–27.

Sambrook Smith GH, Nicholas AP. 2005. Effect on flow structure of sand deposition on a gravel bed: Results from a two-dimensional flume experiment. *Water Resources Research* **41**: W10405. doi:10.1029/2004WR003817.

Sarkar S, Dey S. 2010. Double-averaging turbulence characteristics in flows over a gravel bed. *Journal of Hydraulic Research* **48**: 801–809.

Schmeeckle MW, Nelson JM, Shreve RL. 2007. Forces on stationary particles in near-bed turbulent flows. *Journal of Geophysical Research* **112**(F02003). doi:10.1029/2006JF000536.

Singsabaugh RL, Weiland T, Linkins AE. 1991. Epilithon patch structure in a boreal river. *Journal of the North American Benthological Society* **10**: 419–429.

Smart G, Aberle J, Duncan M, Walsh J. 2002. Measurement and analysis of alluvial bed roughness. *Journal of Hydraulic Research* **42**: 227–237.

Strom KB, Papanicolaou AN 2007. ADV measurements around a cluster microform in a shallow mountain stream. *Journal of Hydraulic Engineering* **133**: 1379–1389.

Strom KB, Papanicolaou AN, Constantinescu G. 2007. Flow heterogeneity over 3D cluster microform: Laboratory and numerical investigation. *Journal of Hydraulic Engineering* **133**: 273–287.

Sumer M, Cokgor S, Fredsøe J. 2001. Suction removal of sediment from between armour blocks. *Journal of Hydraulic Engineering* **127**: 293–306.

Tritico HM, Hotchkiss RH. 2005. Unobstructed and obstructed turbulent flow in gravel-bed rivers. *Journal of Hydraulic Engineering* **131**: 635–645.

Young WJ. 1992. Clarification of the criteria used to identify near-bed flow regimes. *Freshwater Biology* **28**: 383–391.

